SPECTRAL INVERSION TO RESOLVE THIN SANDS AND FAULTS IN THE HITTS LAKE FIELD, SMITH COUNTY, TEXAS

A Thesis Presented to

the Faculty of the Department of Earth and Atmospheric Sciences

University of Houston

In Partial Fulfillment

of the Requirements for the Degree

Master of Science

By

David Mann

December 2012

SPECTRAL INVERSION TO RESOLVE THIN SANDS

AND FAULTS IN THE HITTS LAKE FIELD, SMITH COUNTY, TEXAS

David Douglas Mann

APPROVED:

Dr. John P. Castagna, Chairman

Dr. Evgeni M. Chesnokov

Dr. Rebecca L. Forrest

Dr. Mark A. Smith, Dean, College of Natural Sciences and Mathematics

ACKNOWLEDGEMENTS

I first want to express gratitude to my adviser, John P. Castagna, and also to the members of my committee Evgeni Chesnokov and Rebecca Forrest. I've had the fortune of studying in course work under all of them, and their earnest principles regarding science have shaped me both as a professional and an individual.

My deepest gratitude goes to Carlos Moreno and Gabriel Gil. Their support has made all of the difference in this project.

For help with technical insight, I want to acknowledge Oleg Portniaguine, Firas Jarrah, Stu Fagin, and Charles Puryear. The listed order reflects the chronology of this project, serving as a meaningful reminder to me of when each helped on the way.

For personal and moral support, I owe an immeasurable thanks to my parents Charles and Darlene Mann. When needed, my family was always ready to provide a quiet place to work, and they also expedited my move into a new home, freeing me to spend more time researching.

Last but not least, I wish to thank Maria Vodomirova. As with any project, a great portion of its history will never make it to the page. Maria will help me remember the personal story. As for the facts, you can read them here.

David Mann

Houston, autumn of 2012

SPECTRAL INVERSION

TO RESOLVE THIN SANDS AND FAULTS

IN THE HITTS LAKE FIELD, SMITH COUNTY, TEXAS

An Abstract of a Thesis

Presented to

the Faculty of the Department of Earth and Atmospheric Sciences

University of Houston

In Partial Fulfillment

of the Requirements for the Degree

Master of Science

By

David Mann

December 2012

ABSTRACT

Seismic data are commonly inverted for acoustic impedance in order to image the physical layers of the Earth. However, the thickness of layers relevant to reservoir prospecting is often below vertical resolution. The conventional limit of ¼ wavelength for vertical resolution may be improved using an inversion aided by spectral decomposition. Spectral decomposition decomposes the two-dimensional seismic trace (amplitude vs. time) into a three-dimensional set (amplitude vs. frequency changing with time). Spectral inversion is the process whereby a seismic data volume is inverted for a broader-bandwidth reflectivity of the Earth using attributes calculated from seismically decomposed volumes of amplitude and phase at different frequencies for input. These attributes exhibit a more beneficial interference pattern than traditional reflectivity, and the resulting spectrally inverted seismic survey can be verified using well data from within the survey area. This project uses spectral inversion to enhance the resolution of short-throw faults and Cretaceous sandstones in the Hitts Lake Field, located within the East Texas salt basin. The results are supported using wellbore synthetics and comparison with log-guided fault cutting.

CONTENTS

Chapter 1

Introduction

The vertical resolution of seismic data is conventionally limited to ¼ of the dominant signal wavelength recorded by geophone detectors. This ¼ wavelength is called the tuning thickness, a term which alludes to the disproportionately high amplitude response resulting when reflected waves from the top and bottom of such a layer at this thickness constructively interfere. Below this limit the two events needed to distinguish the resolve the layer are inseparable (Sheriff, 2002). All the same, this amount of vertical resolution has served geophysicists well in locating economic reserves of hydrocarbons within conventional plays such as large, structural traps. However, as newer production increasingly relies upon imaging thin stratigraphy and stimulating existing reserves, so increases the need for vertical resolution in order to minimize risk.

Unfortunately, the successful application of geophysical principles to finding commercially producible hydrocarbons is not always as easy as 'drill the bright spot'. Greater characterization of the reservoir structure is needed for certain producing methods, such as water injection. When a successfully drilled well only yields a small percentage of hydrocarbons judged to be in place, pressure stimulation can be attempted by drilling an adjacent injection well within the same area of connected flow. Predicting where injected fluid will flow requires delineating the reservoir closure on all

sides – either by stratigraphic 'pinch out' or by faulting. The limit to seeing both is the seismic survey's vertical resolution of reflections echoing off of acoustic impedance changes. With the conventional limit of seismic resolution well-established, advances in the field required looking at the seismic response with a new method. Enter spectral inversion.

Spectral inversion is when an accurately defined wavelet is used to invert a seismic volume using its spectral decomposition into time-varying phase and amplitude in order to benefit from the clearer interference pattern and thus derive finer vertical resolution. The first published use of the phrase "Spectral Inversion" was by Partyka et al., (2005). His earlier work discussing thin layer amplitude response (1999) pointed out the inverse relationship between the notch spacing in the frequency domain and the layer's time-thickness in the time domain. Puryear and Castagna (2008) make use of this relationship in their implementation. They discuss the representation of any pair of reflectors as separate even and odd components, which they then relate in the frequency domain to real and imaginary components, respectively, of reflectivity. More recently, Zhang and Castagna (2011) detailed an inversion directly for reflection coefficients in the time domain using a basis pursuit and wedges of even and odd thin layer responses.

Heretofore the literature presenting spectral inversion has been tantalizing, but as with any new technology, real-world applications need to be shown before being readily embraced by the community. This thesis tests commercially offered basis pursuit

spectral inversion and judge its results against well data recorded within the bounds of a given seismic survey over a producing oil field inside the East Texas salt basin.

Figure 1.1. The area of this study is within the Hitts Lake Field, located just North of Tyler in Smith County, Texas.

Chapter 2

Area of Study

2.1 The East Texas Basin

The area of East Texas began to form roughly 200 Ma ago following the break-up of the Pangaea supercontinent. Today, East Texas and the Gulf Coast comprise a tectonically stable region with much thinner crust than parts inland. Its make-up is largely comprised of clastics which were deposited as rivers drained sediments from the continent. The sediments were deposited as sands and muds in geometries influenced by the transgression and regression of the shoreline. The proximity of East Texas to the sea in the later Jurassic and Cretaceous also proved favorable to the deposition of carbonate and salt bodies. The salts, due to their incompressibility, responded with great mobility as the overlaying basin grew. In the surrounding formations, salt movement caused features such as normal faulting, horsts, and grabens. This provided both structural traps for hydrocarbons and also faulting, which in various instances provided fluid transfer or containment. While tectonic features exist on the perimeter of the East Texas Basin, the many fault zones within the basin are attributed to salt mobility, rather than marginal flexure (Jackson, 1982).

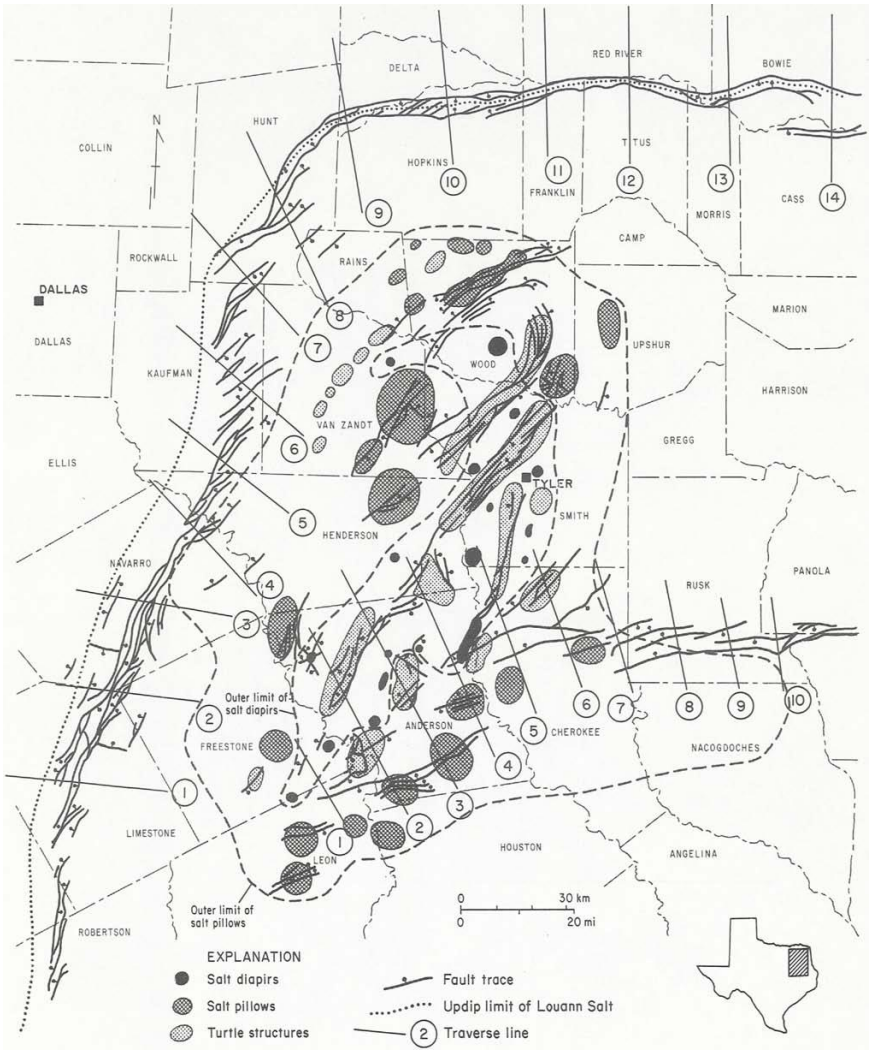

Figure 2.1. The dashed line maps the top of the Paluxy Formation in the East Texas Basin. Clusters of normal faults are associated with salt bodies. From Jackson, 1982.

2.2 The Paluxy Formation

The Paluxy Formation is a lower Cretaceous sandstone and shale package that extends over several states. In East Texas, it sits below the Goodland Limestone and above the Glen Rose Formation. Within the Paluxy, the uppermost sandstone is referred

to as the Paluxy ‘A’, with the next deeper sandstones referred to as the ‘B’ and ‘C’. In the area of this study the ‘A’ sandstone contains commercially producible oil, with the lower sandstones containing brine. Down depositional dip to the South-Southeast, the oil pay terminates into a gas play from the same sandstone. Going west from the region of study, the oils in the ‘A’ sandstone disappear and fresh drinking water is producible. The sandstone reservoirs both within the Paluxy and the similar Glen Rose Formation are thought to have received their oil from the Smackover mudstone in the Upper Jurassic. Hydrocarbons traveled up subsequent faulting and into the sandstone, sealed on top by bounding shales (Schenk and Viger, 1996).

While frequent faulting complicates tracking of the connectivity of the Paluxy sandstones, the stratigraphic responses to electric logs have been well characterized for decades. This helps in well tie correlation with seismic data. Figure 2.2 shows a comparison between electric logs within the Hitts Lake Field and electric logs for a well to the Northeast in Camp County, the latter of which was published by Caughey (1977). Naturally, the Smith County logs show some differences in the more distal depositional setting.

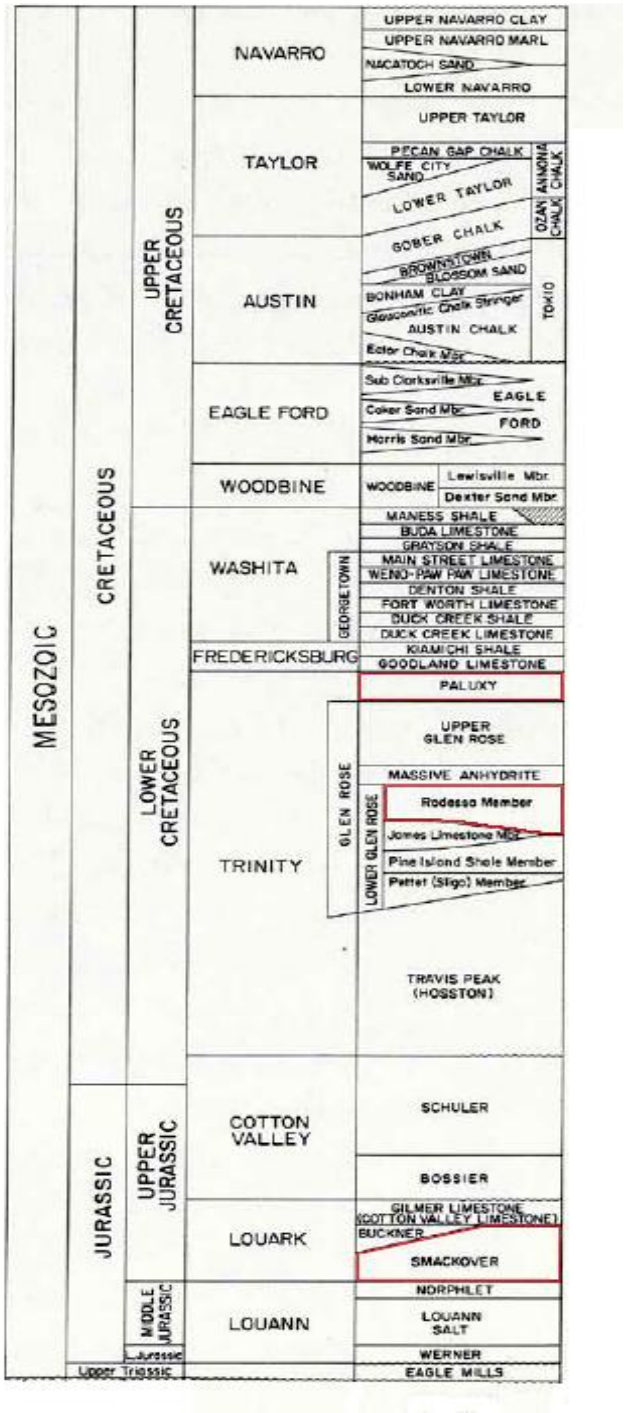

Figure 2.2. The source rocks for the oil in both the Paluxy and Rodessa Formations are located in the Smackover Formation. Modified from Jackson, 1982.

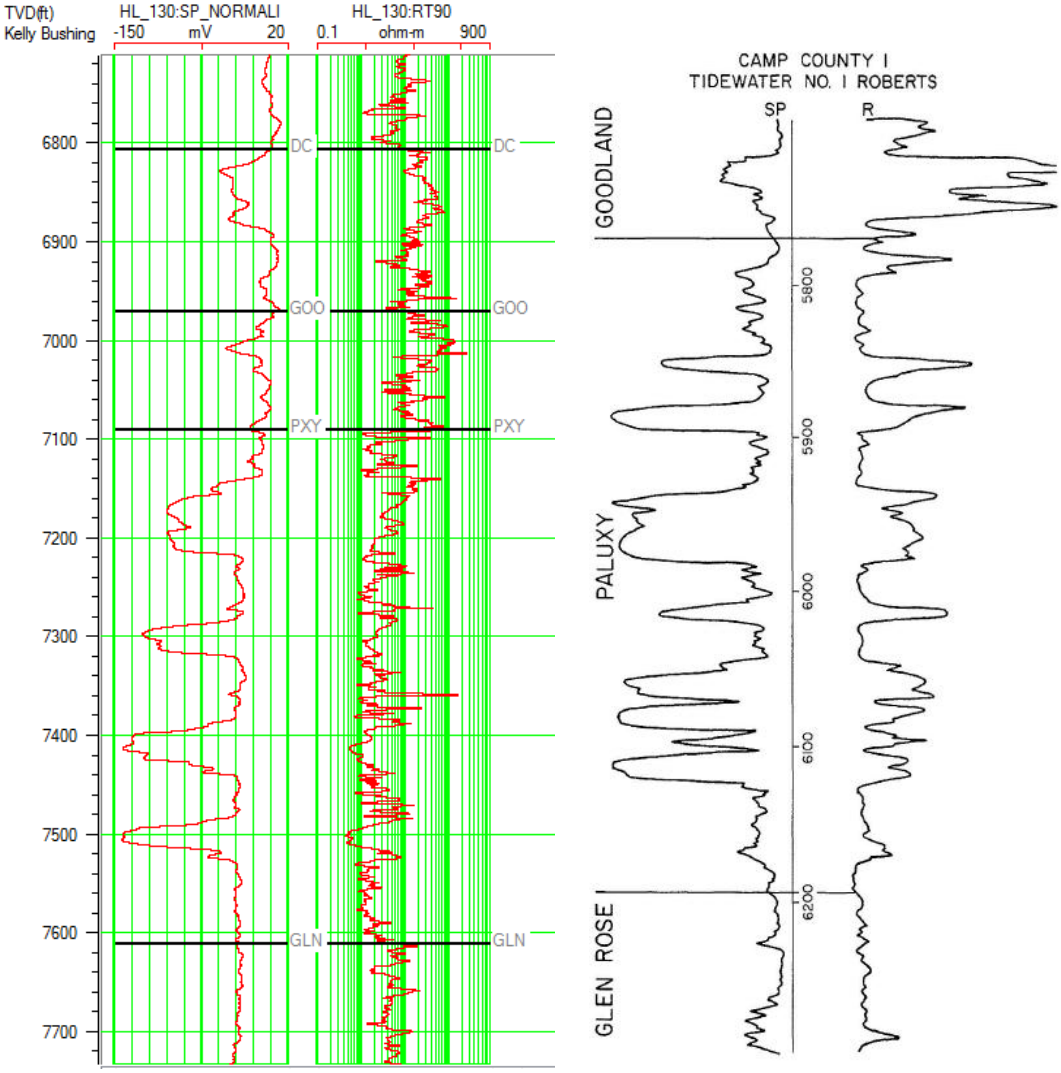

Figure 2.3. Markers were placed at formation tops for every well which had adequate electric log data available. At left is seen logs of spontaneous potential and resistivity for Hitts Lake # 130 well. At right is shown similar logs from Caughey (1977) for a well to the Northeast in Camp county. The Goodland, Paluxy and Glen Formations are abbreviated at left as GOO, PXY, and GLN, respectively.

2.3 The Hitts Lake Field

The area of study for this project is the Hitts Lake Field north of Tyler in Smith County, Texas. The Hitts Lake Field has been producing oil since 1953, and after its first 20 years more 7.6 million barrels of oil were produced (Caughey, 1977).

During the time of the Paluxy's deposition, the area of this survey was an estuary roughly contained by the East Texas embayment (Bigelow, 1991), and the sandstones within the Hitts Lake Field were deposited as distal deltaic sand bars subject to reworking by wave energy.

The dataset used for this thesis consists of a post-stack 3D seismic survey and also log data recorded inside of wells drilled within the same survey area. Fault cuttings interpreted from electric logs were also made available. The seismic data were shot over an area of approximately 9 square miles (23.3 square kilometers) with inline and crossline spacing both at 110 ft (33.53 m). The primary target is the early Cretaceous Paluxy Formation, which sits around 7200 ft. (2195 m) below the surface of the Hitts Lake Field. A secondary target for study was the Rodessa Formation, which sits deeper at about 9300 ft. (2835 m). Within the field, the Paluxy Formation begins with shale on top, which then alternates with two or three sandstones below. Even with high reserves remaining, oil has sometimes failed to produce from the Paluxy A sandstone at commercial rates due to pressure depletion, and so water injection has been used to stimulate production. The choice of injection site is complicated by the fact that the

reservoir sandstone and the frequent faults throughout it are often below vertical resolvability. The Paluxy A sandstones in the region of this study are often 60 ft. (18.29 m) or smaller (Bigelow, 1991). The need for more sophisticated methods is clear as the vertical resolution near the top of the Paluxy in the incoming dataset is over 150 ft. (45.7 m).

Chapter 3

Theory

3.1 Conventional Limit of Resolution

Following a source impulse, perhaps from buried explosives or special vibrating apparatus, ground-coupled geophones record the Earth's internal reflections as amplitude vs. time series called the seismic trace. The seismic trace is customarily modeled as the convolution of the source wavelet with the reflectivity of the Earth's layers. In order to image the physical layers themselves (rather than echoes bouncing off of them), 'removal' of the wavelet's effects is often attempted by inverting the seismic volume for the conducting medium's acoustic impedance.

Unfortunately, the wavelet itself tends to hide information about close events. Consider one discrete layer, such as a sandstone reservoir below the banks of Hitts Lake. The wavelet will see an impedance contrast and reflect a pulse from the top of the layer.

A second reflection will follow once the wavelet reaches the bottom of the sandstone and hits intermediate shale. The resolvability of the two events relies upon the fundamental relationship between the wavelet's dominant frequeny **f**, the velocity of the conducting medium **v**, and the signal wavelength **λ**:

$$V=f\lambda$$

Considering the well Hitts Lake # 122, the given sonic log recorded a compressional wave velocity of 15,034 feet per second (4,582 m/sec) at the interpreted top of the Paluxy Formation at 7,179 feet (2,188 m) below the surface. Using the dominant frequency of 20 Hz, it follows that the signal travels in a wavelength of approximately 752 feet (229 m) within the layer that the sonic velocity reading was taken (assuming constant layer velocity). We have the ability to resolve the top and bottom of this layer only so long as they're separated by 188 feet (57.3 m) or more.

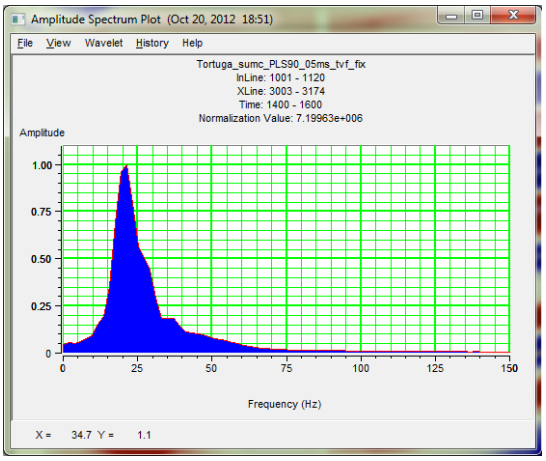

Figure 3.1 The amplitude spectrum of the input seismic shows the dominant frequency here is about 20Hz.

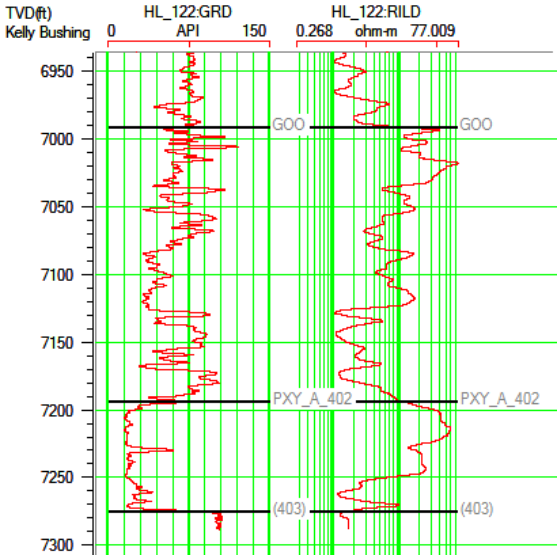

Figure 3.2 The gamma resistivity logs at this well show our reservoir sand spanning 81.5 feet (24.8 m).

In many cases layer thickness can be mapped to the smaller limit of 1/8 of the signal wavelength. This is done using a comparative Wedge model after the work of Widess (1973). In our example here, this means that the correct wedge model could allow us to detect a thickness as small as 94 feet (28.7 m). Unfortunately, the bottom of the oil-containing Paluxy A sandstone has been interpreted from electric logs as sitting at 7,276.5 feet (2,217.9 m), giving us a layer that is about 81.5 feet (24.8 m).

While this thesis does not primarily seek to improve the lateral resolution of the data, it is prudent to know this limit for any interpreted volume. Before receiving the seismic dataset from the operating company, a third-party geophysical company performed the processing, which included 3D Kirchoff time migration. This migration collapsed the diffractions and reflections events to be aligned so that all signal was positioned in time directly below each geophone receiver (known as 'zero-offset' data). Before migration, the lateral resolution was limited by the Fresnel zone. The 3D migration collapsed the signal in both inline and crossline direction. The new limit of lateral resolution is the larger of ½ the illuminating wavelength and the bin spacing of 110 ft. (33.5 m). In our case it is the former, being approximately 375 feet (114.3 m) using the figures from the preceding example of Hitts Lake # 122. Since resolving lateral features depends upon frequency content similarly to vertical features, then one should see improvements to both after applying a method to recover signal bandwidth.

3.2 Spectral Inversion

In the earlier example using well log data at one of the Hitts Lake wells, it was shown that the best case scenario for examining the time-domain reflections still fell more than a dozen feet short of our sandstone. Spectral inversion takes advantage of the characteristic expression of the sub-resolution sandstone's (or any discrete layer's) notch-like response in the frequency domain. Partyka et al. (1999) used this fact to characterize the thickness of a thin layer; the frequency response shows a notch periodicity that is inversely related to the time thickness of this layer in the time domain. Seeing that the superposition of several thin layer responses suggests a non-unique solution leads one to treat this matter as inversion problem.

Resolution was helped further by splitting reflectivity pairs into even and odd components. Any reflection coefficient pair (representing the top and bottom of a thin reservoir, for our purposes) can be decomposed into a pair of an even components and a pair of odd components (Castagna, 2004).

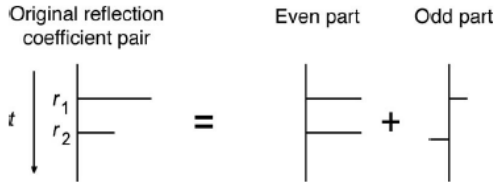

Figure 3.3. Any reflection coefficient pair can be represented as equal-magnitude even and odd pairs, having both positive or opposite polarity, respectively. From Puryear and Castagna, 2008.

The approach of Puryear and Castagna (2008) worked in the frequency domain, associating the even and odd reflectivities with the real and imaginary parts, respectively, of the transformed signal. They then inverted the signal simultaneously for both a series of frequency notch periods and also a reflectivity series. The notch period (in Hz) is viewed as the inverse of time thickness, as treated by Partyka et al. (1999).

The separation into even and odd components allows for the exploitation of the more favorable interference pattern shown in Figure 3.4. The even components of successive reflectors constructively interfere with each other, adding signal on down to zero thickness. The odd reflector pair destructively interferes, going into the noise too quickly as the signal diminishes with decreasing thickness.

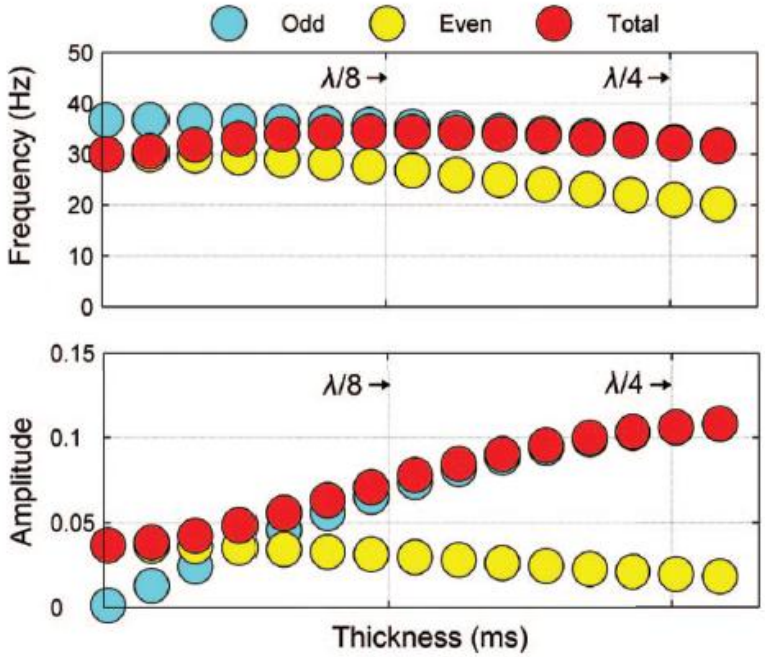

Figure 3.4. The even and odd components interfere in different patterns. This amplitude of the even components increases as layer thickness decreases. From Puryear and Castagna, 2008.

The spectral inversion done in this thesis also decomposes reflectivity into even and odd components, but then it further extends them into even and odd wedge dictionaries. While the specifics of the algorithm are proprietary, it is a time-domain inversion using a basis pursuit of the wedges' reflection coefficient pairs as the component functions that sum together to form the seismic trace. This is essentially a commercial version of the routine proposed by Zhang and Castagna (2011).

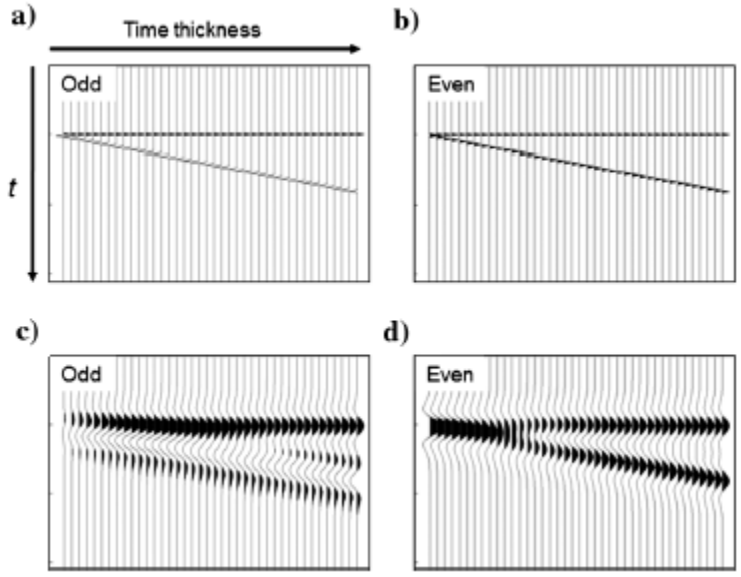

Figure 3.5. Wedge dictionaries are shown for the (a) odd and (b) even components of reflectivity. Their convolutions with a 30Hz Ricker wavelet are shown in (c) and (d). From Zhang and Castagna (2011).

The inversion algorithm in this implementation utilizes a regularization parameter associated with reflector 'sparseness', and it serves as a trade-off factor between resolution and noise. Rather than attempting to qualify this parameter further, this thesis shall follow the lead of Zhang and Castagna (2011) and simply choose the

regularization value that yields the result which looks best against synthetic seismograms.

3.3 Spectral Decomposition

In terms of product, spectral decomposition takes an input seismic time series and outputs a pair of time series – amplitude and phase – at each of several specified frequencies. While the full specifics of how spectral decomposition is employed by this project's time-domain, spare-laryer inversion are proprietary, the sparse layer inversion uses the volumes of spectral decomposition as input in order to take advantage of the frequency-domain signature of sub-tuning thickness layers. Thus at root, the same notch periodicity popularized by Partyka et al. (1999) is used to enhance resolution. Rather than inverting the seismic trace directly, the algorithm can invert volumes of spectrally decomposed phase multiplied by the amplitude of the complex trace's envelope. To best use this phenomenon in order to resolve a thin layer, one needs precision in both the frequency domain so that we can resolve the thin layer thickness, and also in the time domain so we can localize the event so that we know where the thin layer occurs. These two desires, however, are left in competition with one another by the uncertainty principle. This is because the employed short time Fourier transform (STFT) takes places over a specified window. An example window length for the STFT for this purpose would be 40ms. Much work in spectral decomposition has relied upon the STFT. Using a long-

window Fourier transform on our time-domain signal would give us greater precision in the resulting frequency spectrum; however events would be poorly resolved in time. Conversely, choosing a short-window Fourier transform better locates a given event in time, yet our frequency spectrum is less known due to smearing. An alternative approach is the continuous wavelet transform (CWT), which employs a moving time window like the STFT, on the seismic trace is examined for component, best-fit wavelets from a wavelet dictionary. The best-fitting wavelets are subtracted from the windowed signal one-by-one in an iterative fashion until a certain residual threshold is reached.

Mathematically, both the STFT and CWT employ a cross correlation with the windowed portion of the seismic signal – the former with infinite sinusoidal bases in a kernel matrix and the latter with the elements of a wavelet dictionary. In practice, the STFT gets associated with the poor frequency resolution due to smearing, and the CWT with poor time resolution (e.g., we could might accurately predict layer thickness, but not know precisely where in time it occurs). Forgoing both, this project used a newer constrained least-squares spectral analysis (CLSSA) developed by Puryear et al. (2012). As with signal analysis method of the frequency spectrum, the goal is to solve for the Fourier series coefficients. The CLSSA solves for these coefficients directly using a constrained inversion. While the exhaustive mathematics of the inversion isn't laid out here, the inversion begins with the modeled forward equation:

$$\mathbf{Fm = d}$$

Where **F**, **m**, and **d** are, in order, the kernel matrix of sinusoidal bases, the Fourier series coefficients for which we wish to solve, and the windowed seismic trace (Puryear, et al., 2012). Assuming the sinusoidal basis elements of F captured inside the window were not correlated, the normal equations of linear inversion

$$\mathbf{F^{*}Fm = F^{*}d}$$

would be considered adequate for a solution. As Puryear et al. (2012) point out, however, the windowing of the data itself means that the sinusoidal elements are correlated. The normal equations lead to a unique solution with the addition of constraints, namely weighting matrices W_m for the Fourier coefficients (model parameters) **m** and W_d for the windowed seismic data **d**. The equation to solve becomes

$$W_d F W_m (W_m)^{-1} m = W_d d$$

The inversion is handled with user-definable regularization for stability of the solution, and the weighting values of W_m changes with iteration. Puryear et al. (2012) give several synthetic and real examples which show frequency and temporal resolution using CLSSA superior to both the STFT and CWT.

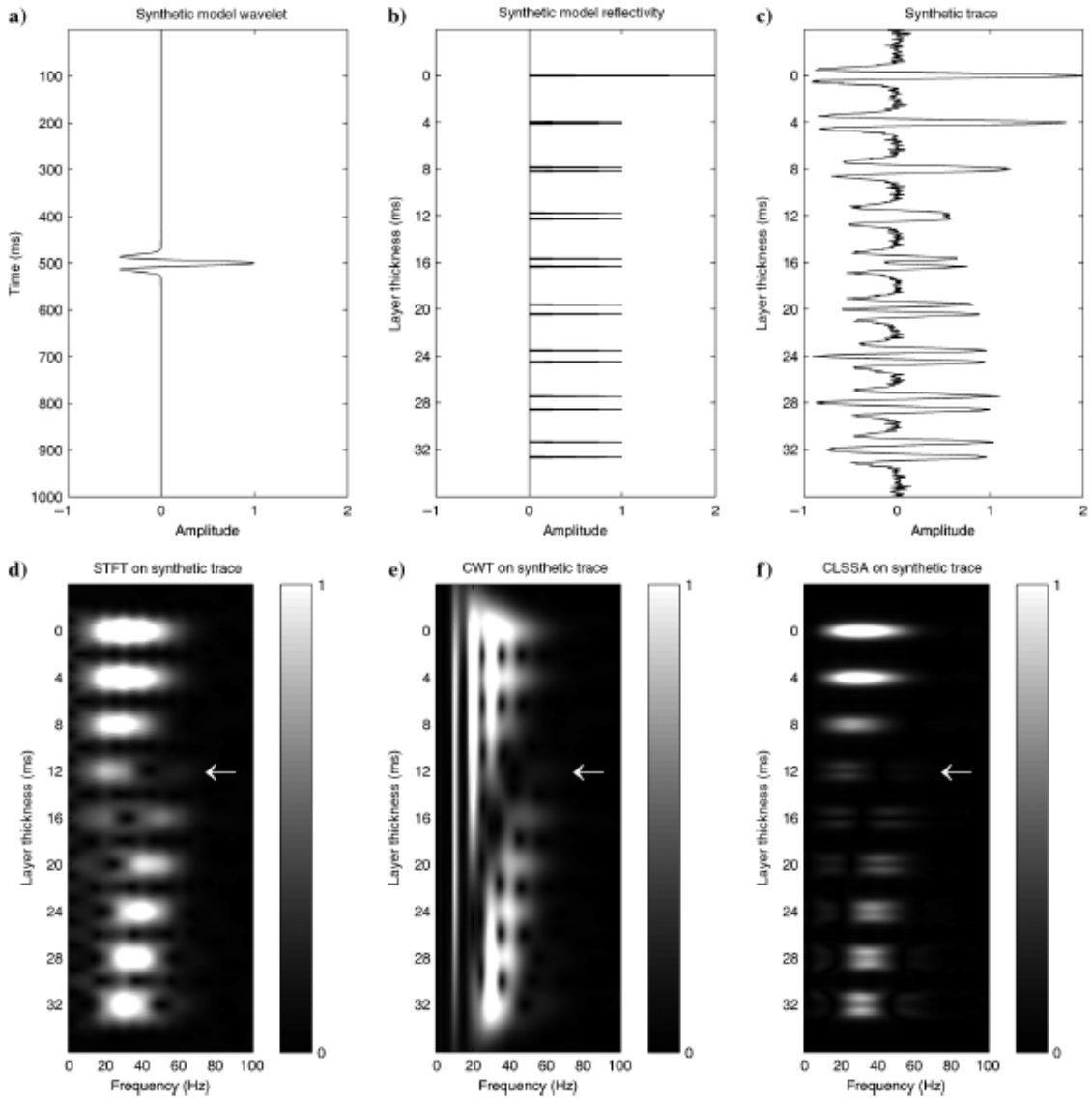

Figure 3.6. The above image (c) shows the resulting trace of the wavelet in (a) convolved with the layer reflectivity in (b). In the bottom row, three attempts are made to transform the seismic signal of (c). Finer resolution is achieved by the CLSSA (f), where the Fourier series coefficients are solved for using a constrained inversion, rather than a projection of sine waves assumed to be orthogonal (d) or an iterative subtraction of elements in a wavelet dictionary (e). From Puryear et al. (2012).

Chapter 4

Methodology

4.1 Workflow to Invert Volume

A three-dimensional seismic survey will be spectrally inverted in the time domain using volumes of spectral decomposition and a known wavelet. The spectrally inverted result will be a volume of high-resolution reflectivity, meant to be an interpretable model of the Earth that has the destructive properties of the wavelet removed.

Seismic energy becomes band-limited as its travel through the Earth attenuates the lowest and highest contained frequencies, and so the relative peaks and troughs of the seismic signal cannot yield absolute values of reflection strength unless the volume is 'calibrated' to another type of data such as well logs. This is the procedure typically followed when inverting a seismic volume for another value, such as acoustic impedance, which takes it basic mathematical relation from the convolutional model and uses well-log derived impedance for starting input 'solutions'. When a well is drilled, two of the many physical properties that can be measured are elastic wave velocity and density. Commonly called a sonic log and density log, respectively, their product yields acoustic impedance, to which seismic reflectivity is directly related. There are two major differences in what is done in this thesis. Instead of acoustic impedance, the inversion result will be a volume of reflectivity with an increased amount of bandwidth in the frequency spectrum recovered from what was originally lost in the Earth. Secondly, after

Zhang and Castagna (2011), we will not use well-derived reflectivity as a starting solution (although it is possible in principle). Instead, the inversion is a basis pursuit of wedge dictionaries. However, well data will be used in this thesis in order to accurately verify the source seismic wavelet which interacts with the reflectors. The correct estimation of the wavelet is the most crucial input to spectral inversion. The software algorithm employed expects a volume at 0◦ phase, so the initial workflow focuses on cleaning the seismic volume and verifying its phase using well data.

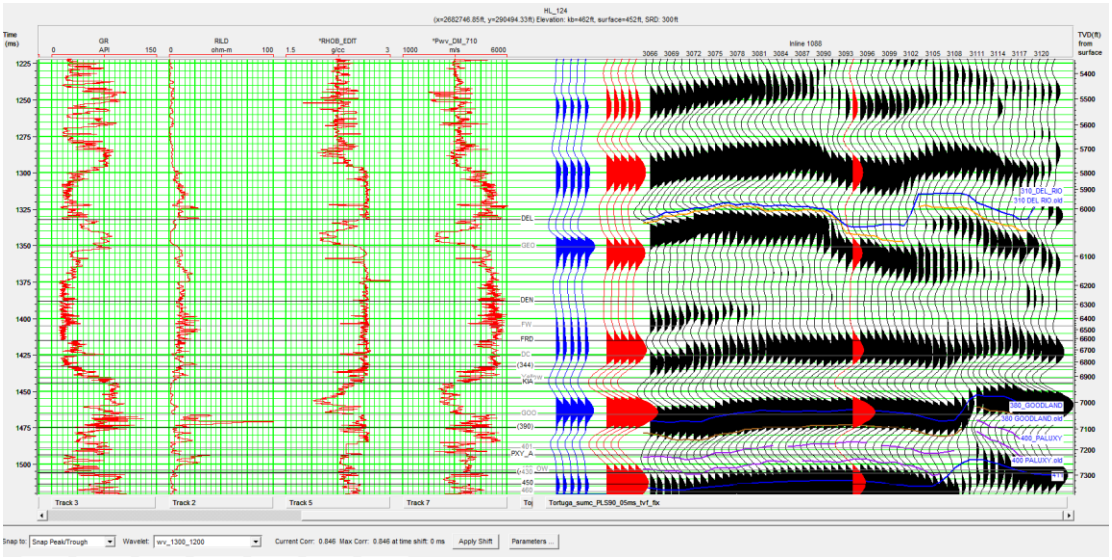

Figure 4.1. A typical example of a well-tie is shown here. The synthetic signal (blue) is calculated using density and sonic log data from the well. The composite trace (red) is generated from seismic traces (black at positions close by the well. At the discretion of the interpreter, minor changes can be made to the synthetic trace so that it best correlates with the real seismic volume in terms of depth and time. While the logging data sees finer detail, the correct choice of wavelet will yield a synthetic with only as much detail as the seismic.

The incoming seismic survey will be conditioned by 1) first cleaning the spectrum for noise using a time-varying bandpass and 2) applying a structural filter in order to

boost the signal to noise ratio. Next the conditioned seismic volume will be correlated with wellbore synthetics. This will verify the wavelet for purposes of inversion, and also allow for the volume to be phase rotated as necessary to situate the reflective peaks directly over the reflecting impedance events. This last condition, referred to as 'zero phase', centers the bulk of the reflected signal energy precisely at the reflector. To a physicist, this may seem counterintuitive, since the leading side lobe of the reflection arrives in time before the reflection event itself. More intuitive might be a causal wavelet, where the bulk of the energy shows up in time slightly later than the amount of travel time needed for the echo to move from the reflecting layer up to the geophone sitting on the ground. This representation, similar to that used by seismologists studying an earthquake, is referred to as 'maximum phase'. The other extreme of the convention would show the bulk of the reflect energy coming sooner than the event, referred to as minimum phase. Zero phase is the industry preference for interpretive seismic geomorphology, since reflection 'events' can be associated with strong amplitudes used to spot them visually.

4.2 Method to Verify Results

Considering a dominant frequency of approximately 22 Hz in the seismic data, the conventional standard of ¼ wavelength yields, using logged velocities near one well, a vertical resolution of 152 ft (46.3 m). near the Paluxy Formation and 181 ft. (55.2 m) near the Rodessa.

This thesis worked upon the following hypotheses:

1) The applied spectral inversion on the seismic volume will improve vertical resolution and correlate well with events appearing on well-log control.
2) Applying spectral inversion to the volume will allow for the detection of faults with a throw smaller than the vertical resolution of the seismic data.

The motivation for both is to provide clear insight into reservoir connectivity and allow for better planning for both further well placement and also for hydraulic stimulation. In order to verify the first point, the spectrally inverted result will be compared with wellbore synthetics, allowing the reader to make a visual judgment regarding goodness of fit. This will be limited to well locations where both sonic and density logs are available, totaling about 7.

As for verification of improved fault resolution, the spectrally inverted volume will be compared with interpreted fault cutting mapped from well logs. Fault cutting has been mapped at 49 well locations, many of which are below vertical resolution.

For verification of the first hypothesis, the synthetics will be generated using wavelets statistically extracted from the seismic data in the CGG Veritas software eLog. An extraction window is set for 1000ms-1500ms. While the top of the target Paluxy Formation begins near 1500ms for most wells, it is desired to extract the wavelet over a portion of logged hole. Since most sonic and density logs end shortly after the Paluxy is reached, the wavelet extraction window is started higher at 1000ms, providing two and a half times the length of the 200ms wavelet. The window should be no shorter than twice the length of the desired wavelet.

Chapter 5

Results and Discussion

5.1 Data Conditioning

This will explain every step taken after receiving the post-stack volume from the client. The nature of the spikey-edged noise will be described, as well as the filtering applied.

The conditioning applied to the data can be separated into two parts: frequency spectrum and noise. The frequency content of the seismic was examined by extracting a time-varying wavelet and watching the change in its amplitude spectrum with increase in travel time. The layers of the earth serve as excellent filter for high frequencies, and so it was assumed that the time-varying spectrum would have its broadest point shallow, and then decrease afterwards. To examine the noise of this volume, a time varying, zero-phase wavelet was extracted from the volume. The spectrum is seen is in Figure 5.1. The observed energy outside of the main trend was judged to be noise, and so the parameters of the time-varying bandpass filter were chosen. The cleaned result after filtering is shown in Figure 5.2.

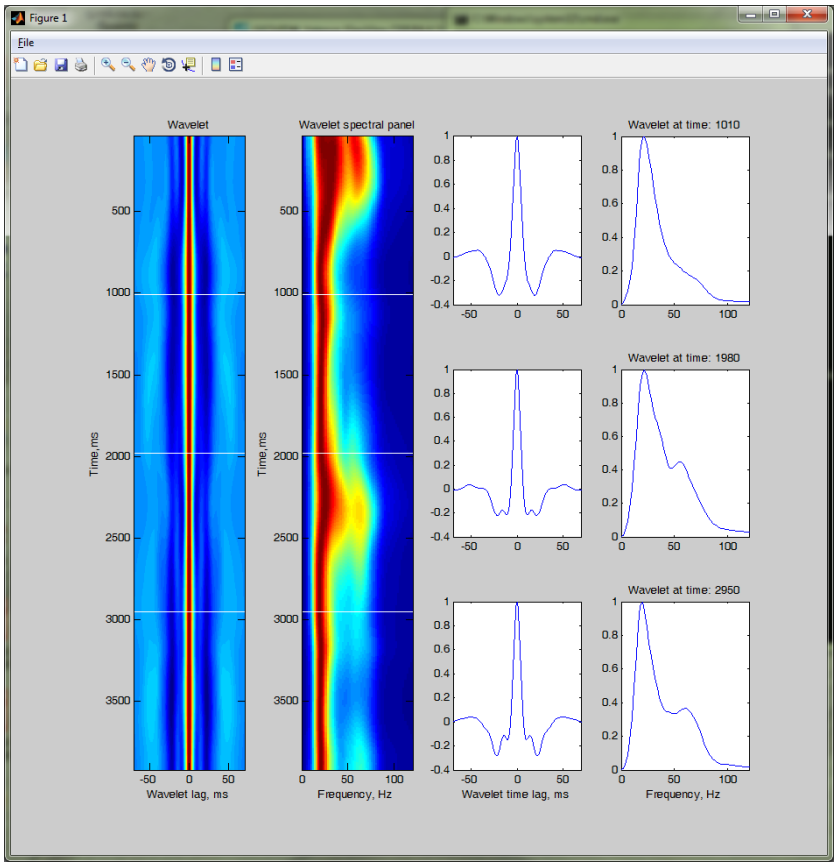

Figure 5.1. Above is shown statistically extracted, time-varying wavelet before from the raw data volume .The uneven, higher frequencies are interpreted as noise, given that one expects frequency content to decrease.

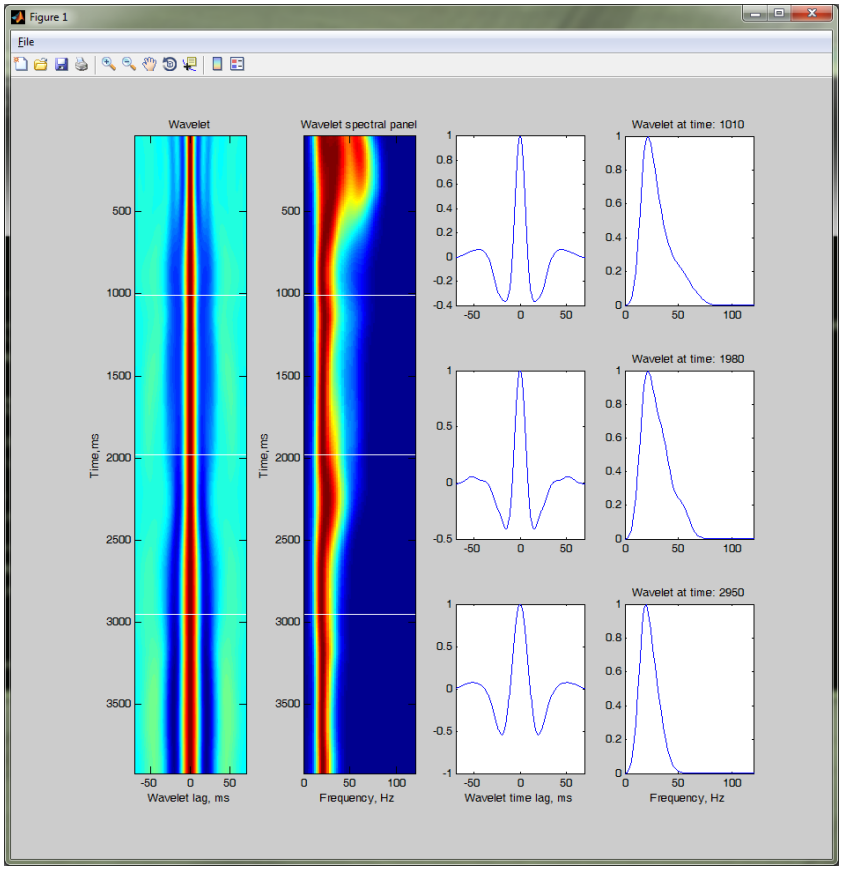

Figure 5.2. Above is seen a time-varying wavelet over the four second volume after a time-varying bandpass was applied. The sidelobes have been noticeably cleaned of noise.

After the spectrum was cleaned, attention was turned to the greatest challenge with this dataset: the noise. A time slice of the volume's amplitude shows highly lineated noise, and to further complicate matters, vertical sections regularly showed upward and downward-pointing spikes.

Applying a rigorous structural filtering regimen, however, posed a real problem: there was a possibility that legitimate faulting could be lost in the course of smoothing out systematic noise. In order to preserve as much information as possible, three-

dimensional scale decomposition split the volume into seven component volumes. The volumes are generated by a grid subtraction of elements falling within a unit grid space with dimension equal to 2^n traces, where the term n is the scale number. The process is dynamic, so that if no coherent energy remains within the grid of unit size 128 (2^7) traces, then there will be no seventh volume. The set of scaled volumes recombine, via arithmetic sum, into the original volume. This method is appropriate for treating noise of a systematic nature, and here it allowed for the noise to be filtered separately according to the needs of each scale.

Upon examination of the different scales, it was decided that noise should only be treated in scales 01 and 02. Filtering was provided using a three-dimensional, fault-preserving structural filter. The variable input parameters to this process were aperture size, number of iterations, and a fault-preserving threshold. In the opinion of the author, the last part was the primary strength. For the final volume, it was lowered from the present versions default of 3 to 2.

For quality checking, a residual volume was generated by taking the arithmetic difference between the raw volume from the client and the volume after frequency and noise filtering. Making sure that no coherent signal has been filtered away typically means that only random noise is seen in the residual. Examined up the inline, there was some coherent layering in the residual. However, this was expected due to the nature of the filtered footprint: higher amplitude concentrated along survey inlines. So the success of the filter was primarily judged orthogonal to this, being along the crosslines.

Figure 5.4 Shows the residual between the filtered result and the original volume as indeed only noise and not geology.

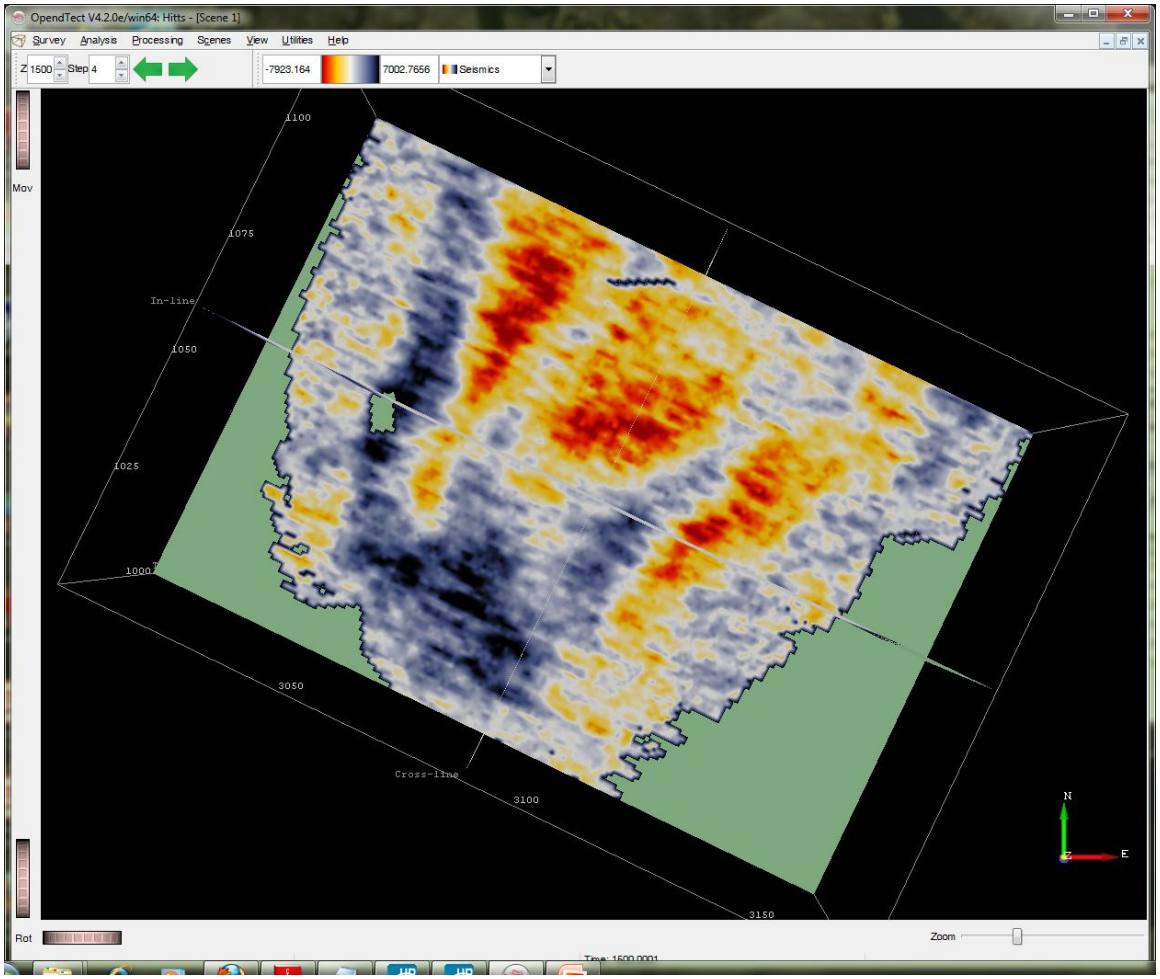

Figure 5.3. Above is seen a time slice of the seismic survey at 1500 ms. The highly lineated acquisition footprint (running Northwest to Southeast) proved challenging to deal with. Noise remained in the final results despite substantial improvement after noise filter. Ultimately, a noisier final result was generated in order to see more faulting.

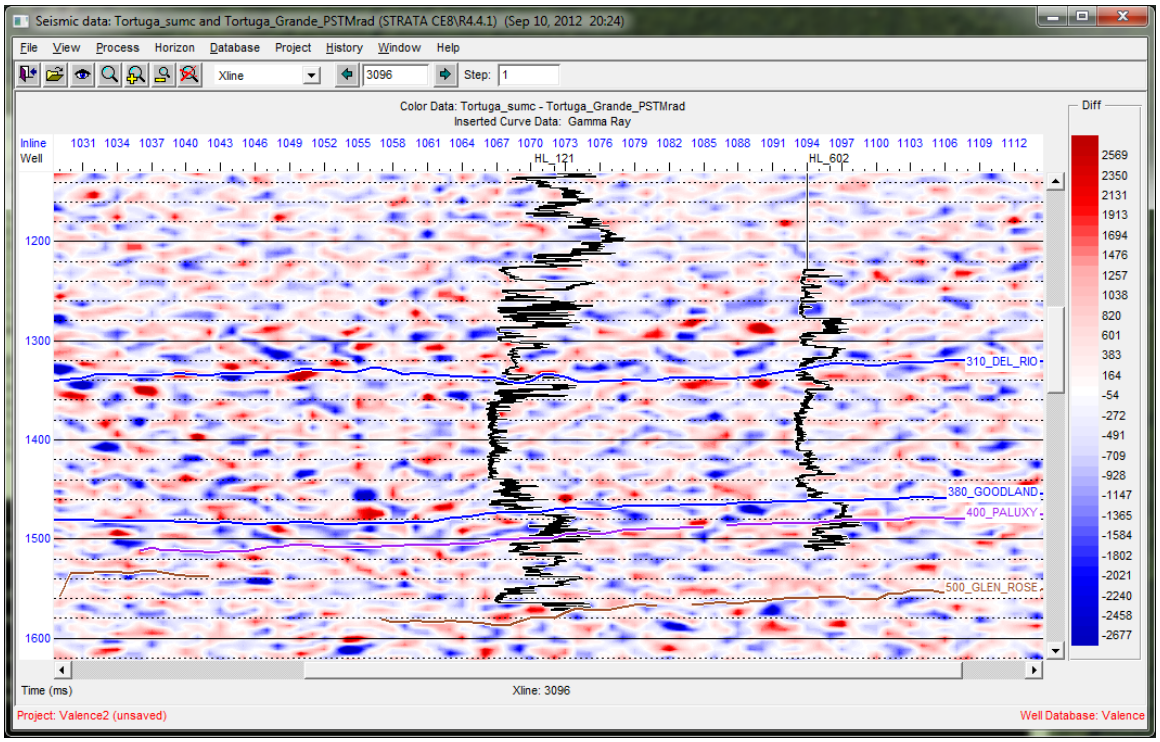

Figure 5.4. A vertical section is shown along crossline 3096. To aid in searching for coherent structure, gamma log plots are inserted at well positions, and mapped horizons are also shown. The purely random nature of the above is an indication that no coherent signal related to geology was removed from the original volume.

5.2 Phase Calibration using Well Logs

The well data available allowed for the determination of the seismic data's phase, or in other words, the phase of the wavelet created by the seismic survey's source and convolved with the Earth's reflectivity series. Even though the wavelet's phase can change across the study area, this project considered the seismic to have only one constant phase for purposes of interpretation. In order to determine the phase of the dataset's wavelet, synthetic well logs were generated from velocity and density data recorded inside of wells drilled within the study area. At any given time within the

software used, a percentage correlation value between the synthetic and composite trace was given.

Once an initial tie between the synthetic and seismic was achieved, two geological zones were used for scanning the phase: the Del Rio Shale, and the Paluxy Formation.

	HL 124	HL 122	HL 602	HL 129	HL 125
Del Rio Shale	-84	-100	+104	-32	-23
Paluxy Fmn.	-109	-114	-4	-81	-168

Table 5.1. Across two different geological formations at each of five wells, the software found the maximum correlations with seismic by rotating the wavelet the amounts listed above. For purposes of interpretation, the volume was treated as having a single wavelet with -90 phase rotation. Well # 130 was not logged over the Del Rio interval. Well # 121 wasn't included here given the patchiness of its logs.

Since figures around -90 were dominated the results, the seismic volume was considered to be -90 as a whole and a +90 phase rotation was applied to the volume.

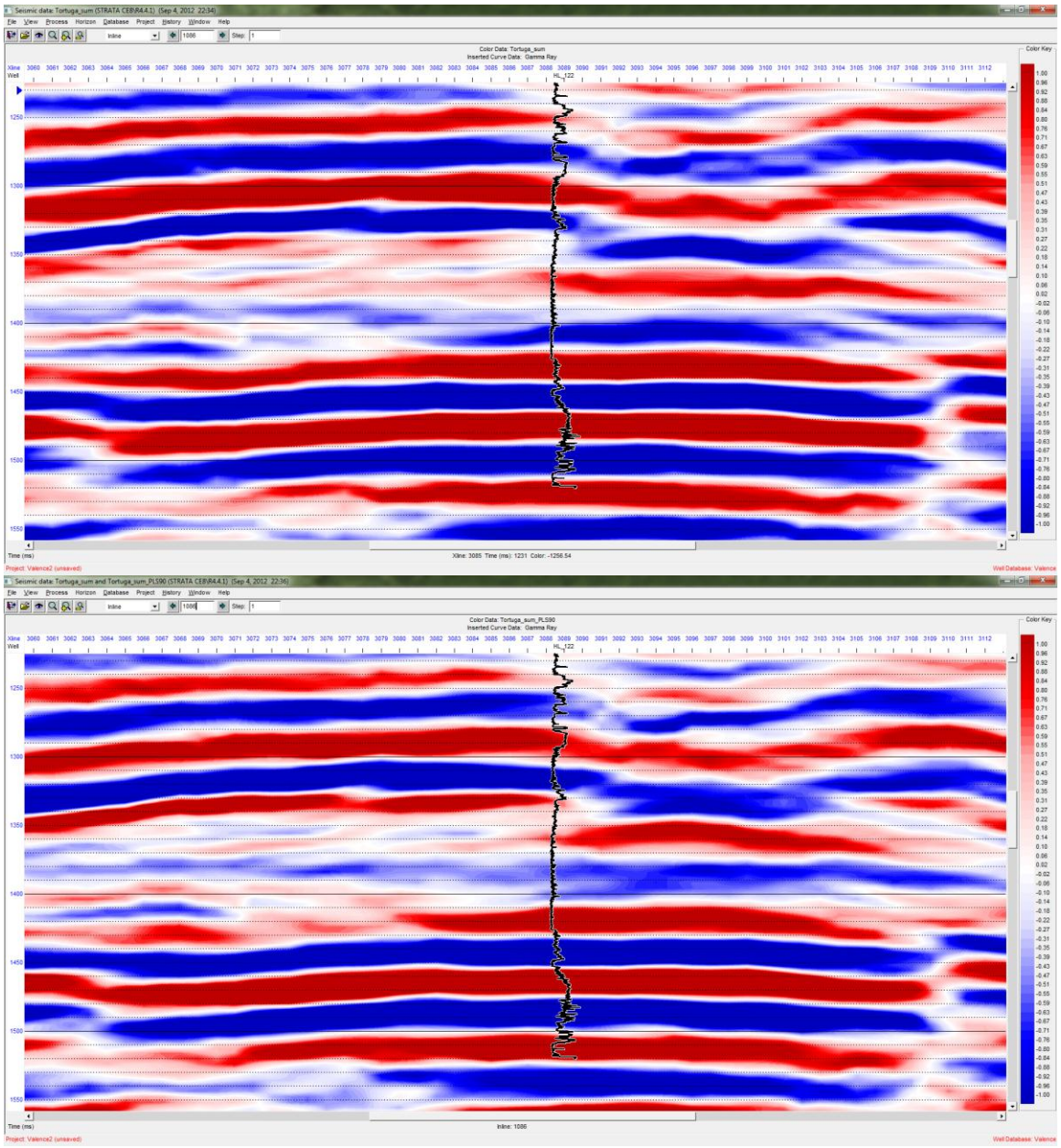

Figure 5.5. Shown are vertical sections of the seismic volume before (above) and after (below) a +90 phase rotation was applied. The gamma log at the location of well HL 122 is inserted. The phase rotation is evidenced by the fact that gamma readings which previously sat on zero crossings (in white) now either sit on peaks or troughs.

5.3 Spectral Decomposition

After conditioning and calibration (rotation) of the seismic volume to zero phase, the amplitude spectrum was examined to choose limits for decomposition. I chose the main bounds of the spectrum limits as 10-45 Hz, and then generated a time series for each of amplitude and phase at every 5 Hz of frequency data (a total of 16 volumes).

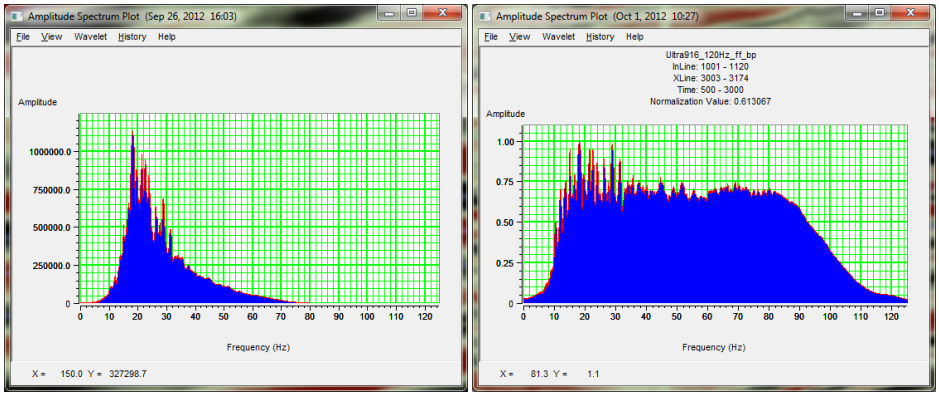

Figure 5.6. The spectrum of the conditioned seismic volume is shown above at left, with that for the Ultra™ result shown at right. The spectral decomposition was performed from 10Hz to 45Hz, analyzing the majority of the signal from the conditioned seismic.

5.4 Spectral Inversion

The spectral inversion was judged a success since the well log synthetics yielded favorable correlations. While some type of log data was available for 50 wells, only 7 wells had both sonic and density logs recorded. At most well locations, the correlation window was limited by the overlap between the sonic and density logs. For the most

part this covered the same geologies. Other wells, particularly Hitts Lake # 129 and Hitts Lake # 130, covered a much deeper extent. Their windows were set to comparable lengths as for the other wells. The correlations are summarized below.

Well #	Seismic	SI	SI/Seismic	Correlation Window (ms)	Window (ms)
121	0.877	0.302	0.344	1150-1552	402
122	0.859	0.345	0.402	1200-1512	312
124	0.856	0.464	0.542	1221-1524	303
125	0.818	0.445	0.544	1235-1500	265
129	0.822	0.447	0.544	1300-1650	350
130	0.766	0.357	0.466	1480-1800	320
602	0.919	0.480	0.522	1200-1515	315
Average	0.845	0.406	0.481	-	323.9

Table 5.2. The results for synthetic well correlation are summarized. A synthetic seismogram was generated at each well for both the seismic and spectrally inverted volumes. The wavelets used were statistically extracted.

The correlation coefficient for the spectrally inverted well ties is on average half of that for the seismic well ties. In the author's experience, this is typical for spectral inversion project. There are two reasons suggested for this. Firstly, it is generally harder to match broader bandwidth than narrow bandwidth. Narrow bandwidth means that the extracted wavelet generates a synthetic with more detail, and thus a stricter test as to whether or not your synthetic agrees with the traces from the volume. Secondly, only higher frequencies are recovered by the inversion. Thus, the well log synthetic with the higher resolution wavelet will contain more low frequency content than the spectral inversion itself, leading to a lowered correlation.

Examined both in vertical section and in time slice, the spectrally inverted volume shares the same large-scale structure as the conditioned seismic, so it is obvious to the viewer that they belong to one another. The biggest difference is the increased layering in the inverted volume.

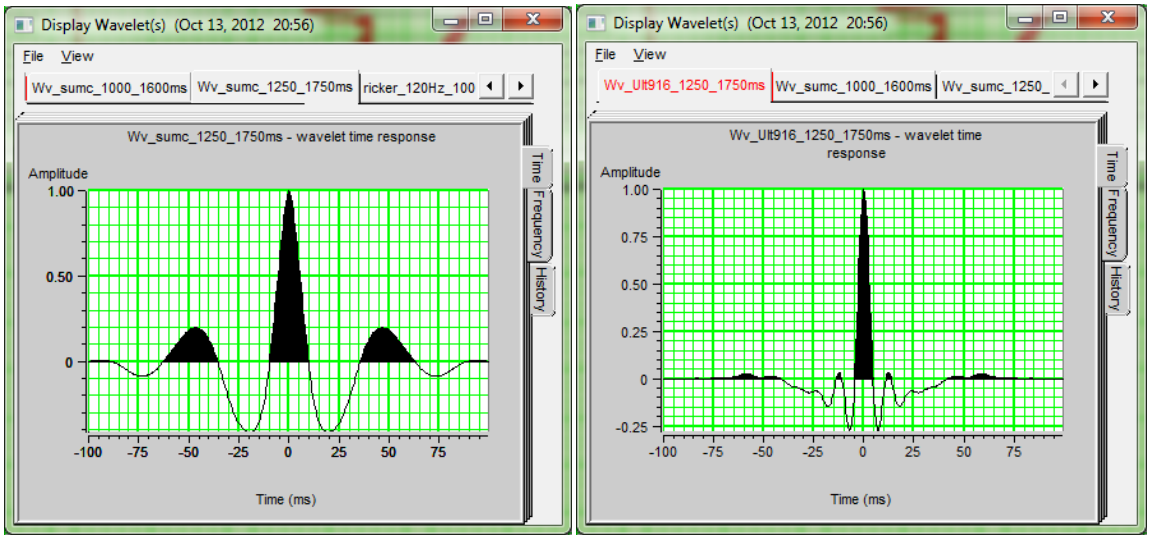

Figure 5.7. The statistically extracted wavelets for the seismic (left) and spectral inversion (right) are shown here. Inverting the time between central troughs, the wavelets have dominant frequencies of approximately 25 Hz and 67 Hz, respectively. Other references of dominant frequency herein refer to the peak amplitude of the seismic data's spectrum.

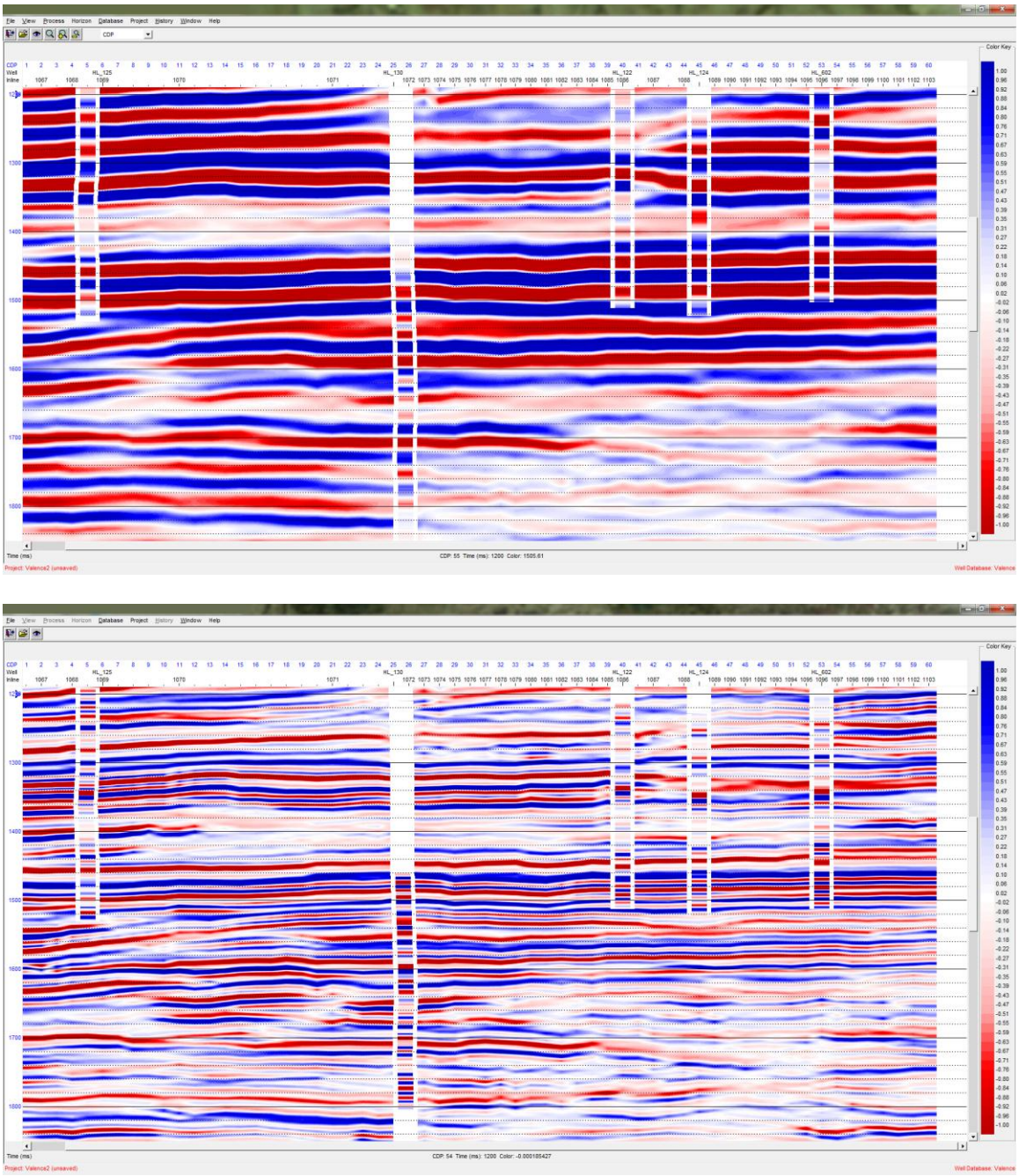

Figure 5.8. The same vertical section across an arbitrary line is shown for both the conditioned seismic (above) and the spectrally inverted result (below). The inset at each of the five well locations shows well-derived reflectivity convolved with a statistical wavelet respective of the volume.

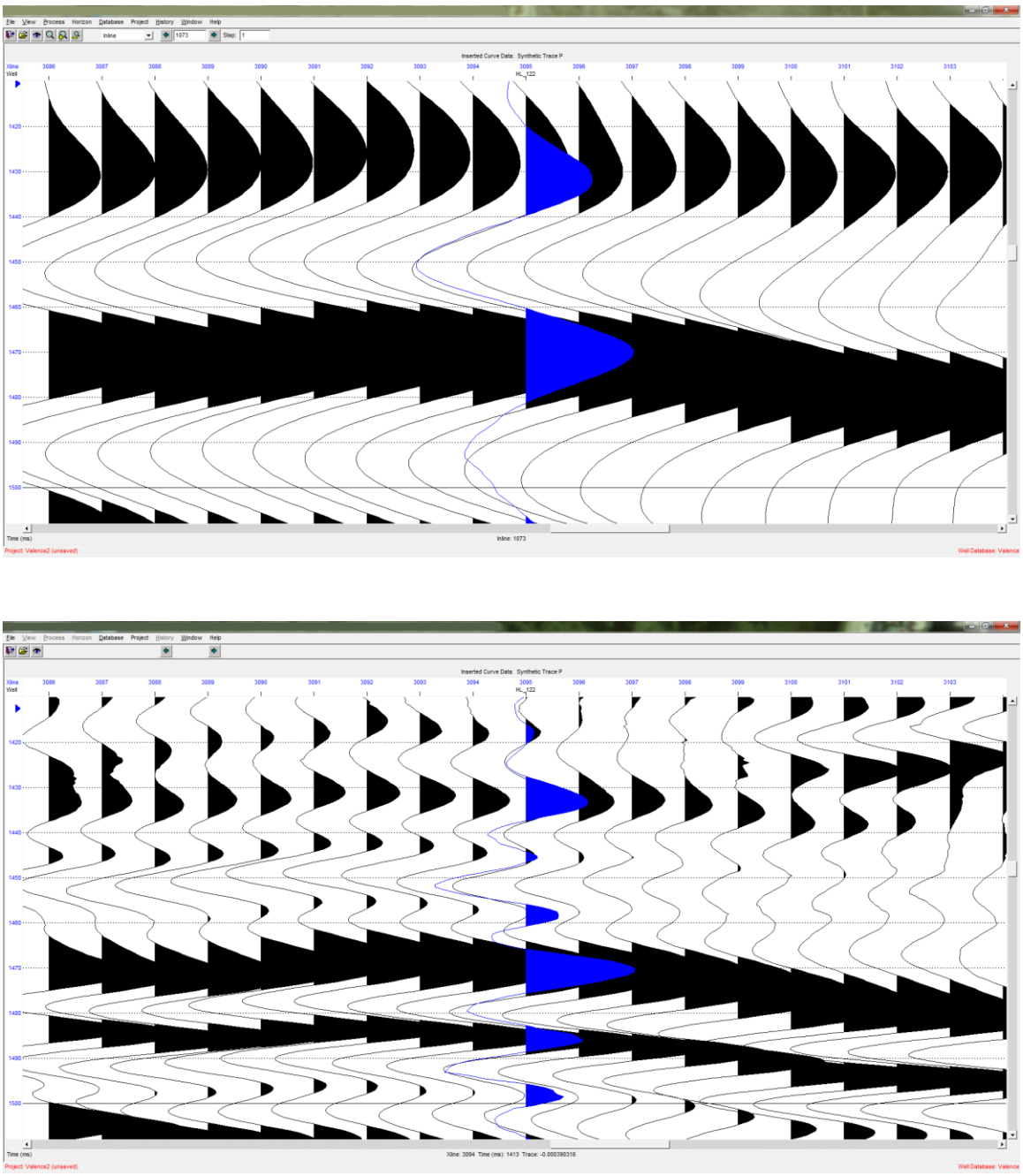

Figure 5.9. At the location of Hitts Lake well # 122, a wellbore synthetic is shown in blue for conditioned seismic (above) and also the spectrally inverted volume (below). The wavelet for each is statistically extracted from the respective volume, for which the traces are shown in black.

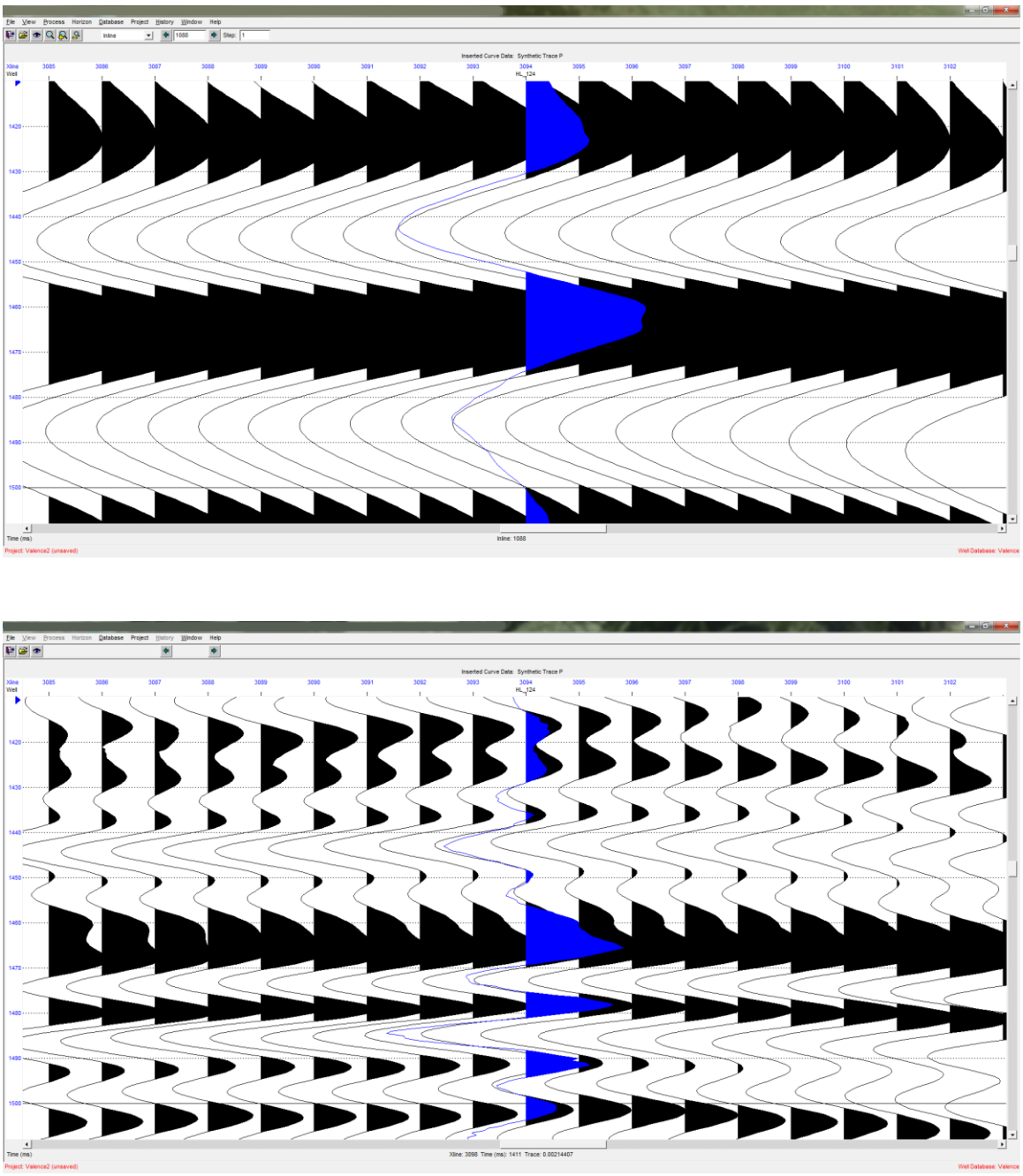

Figure 5.10. At the location of Hitts Lake well # 124, a wellbore synthetic is shown for conditioned seismic (above) and also the spectrally inverted volume (below). The wavelet for each is statistically extracted from the respective volume.

Addressing the second hypothesis for increased fault resolution was open to greater subjectivity. The spectrally inverted volume definitely showed increased breaking which resembled plausible faulting in principle. Judging whether the faulting was recovered or noise wasn't as simple as looking for breaks which extended across multiple lines; this area is known for faulting on the order of and smaller than both the bin spacing and improved resolution.

Since extensive stratigraphic picking and fault mapping from electric logs at 49 well locations was available, the decision was made to examine every well location for any breaking consistent with mapped faults. In the first pass, a table listing all of the fault cutting in measured depth, start and end time was used. In this way, the spectrally inverted volume was examined without the visual bias of the log-mapped fault lines being displayed. For agreeable breaking which was spotted on the inversion, its row on the table was marked. These good candidate wells were then examined with the log-interpreted faulting displayed.

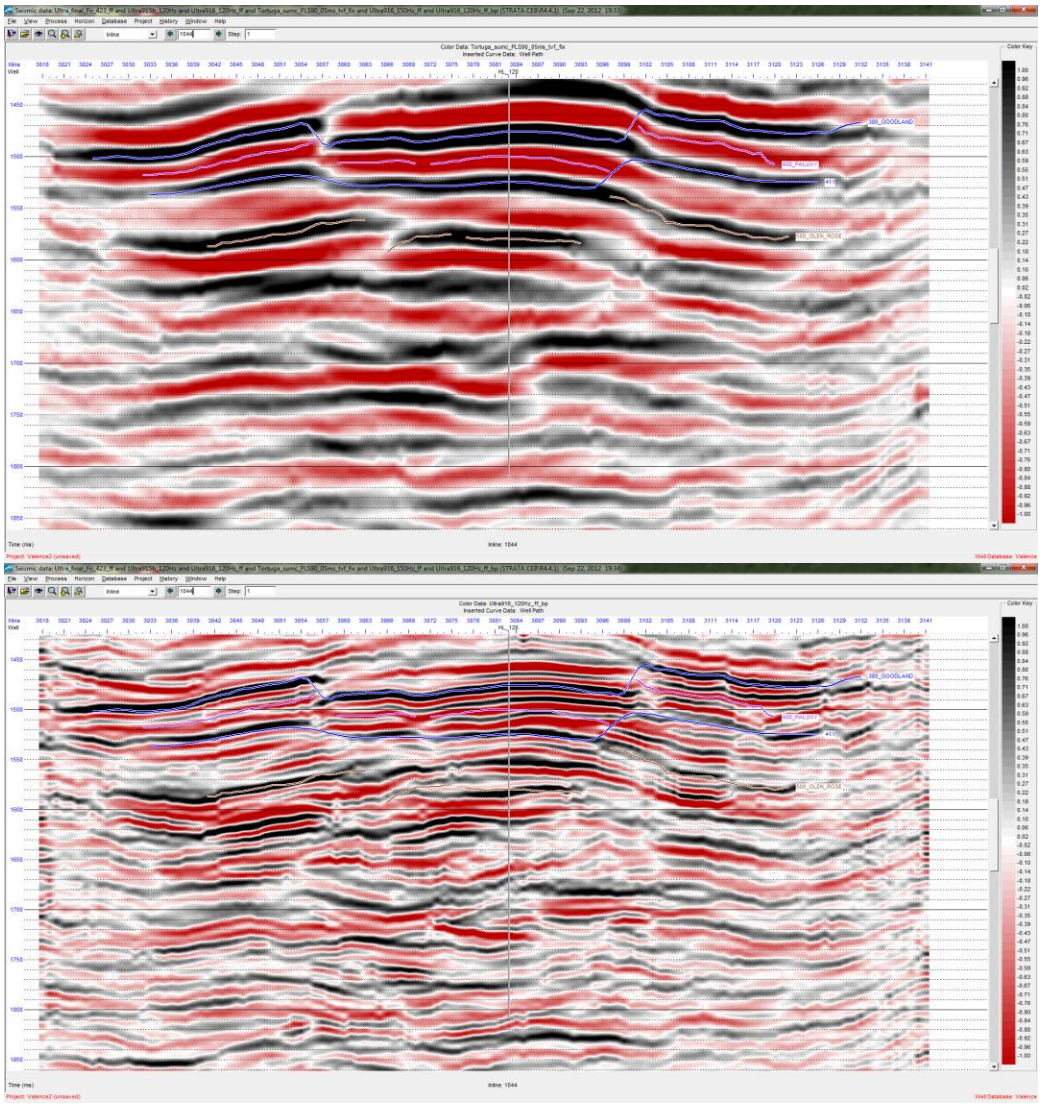

Well	Elev.	Depth(MD)	Throw	Top Time	Bottom Time	Abbrev
HL_120	448	6410	106	1.38797	1.40271	HL_SH_02
HL_120	448	7503	53	1.54373	1.55421	HL_PX_15
HL_120	448	7978	14	1.63015	1.63242	00_20
HL_120	448	8249	6	1.67476	1.67573	00_20
HL_120	448	8417	30	1.70007	1.70493	HL_DEEP
HL_120	448	8583	176	1.71515	1.7437	HL_PX_03
HL_120	448	8881	11	1.77688	1.77866	00_20
HL_120	448	8960	5	1.79018	1.79099	HL_DEEP
HL_120	448	9017	38	1.79675	1.80291	HL_PETTET_04

Figure 5.11. A tabled list of faults and throws was used to examine the results without the bias of mapped fault lines displayed. The faults which agreed in position and throw are marked in black above. Here, the fault starting at 1.38797ms is above the current view window.

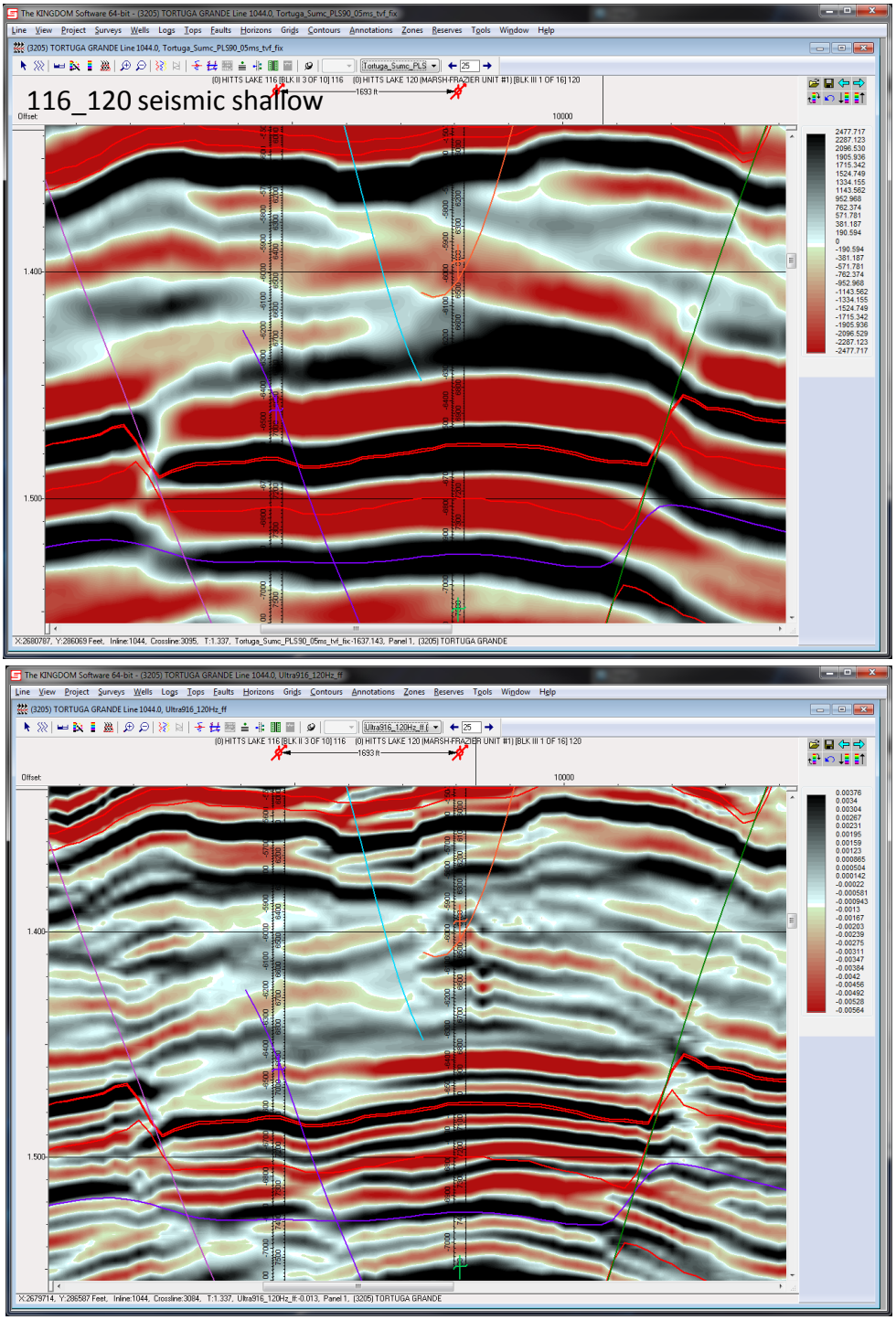

Figure 5.12. The same vertical section is shown for seismic (above) and spectral inversion (below) with wells # 116 and #120. Note the previously unresolved faults crossing well #116 at 1454ms, and especially crossing well #120 near 1400ms.

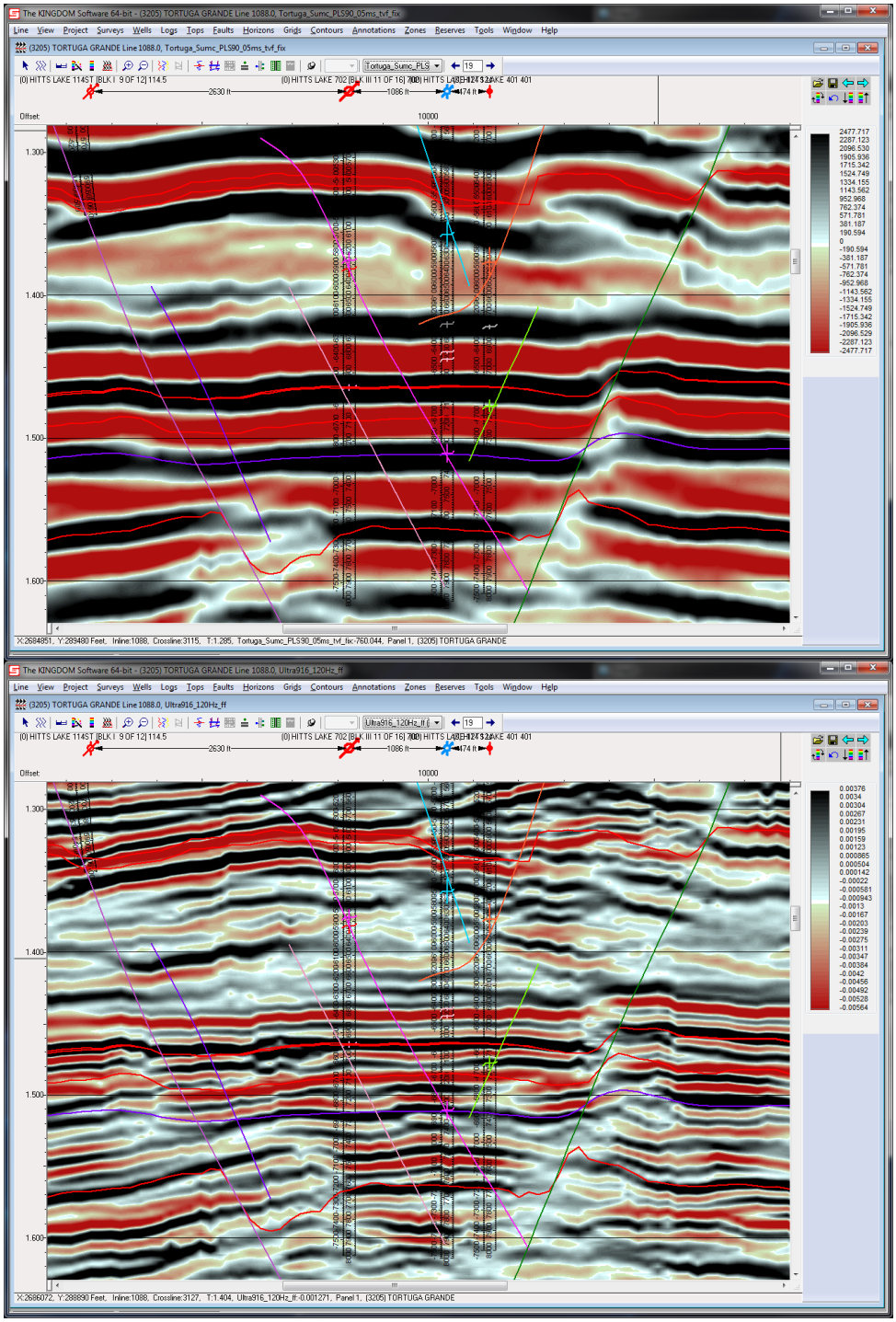

Figure 5.13. The same vertical section is shown for seismic (above) and spectral inversion (below) with wells #702, #124, and #401. A closer view is seen in the following figure.

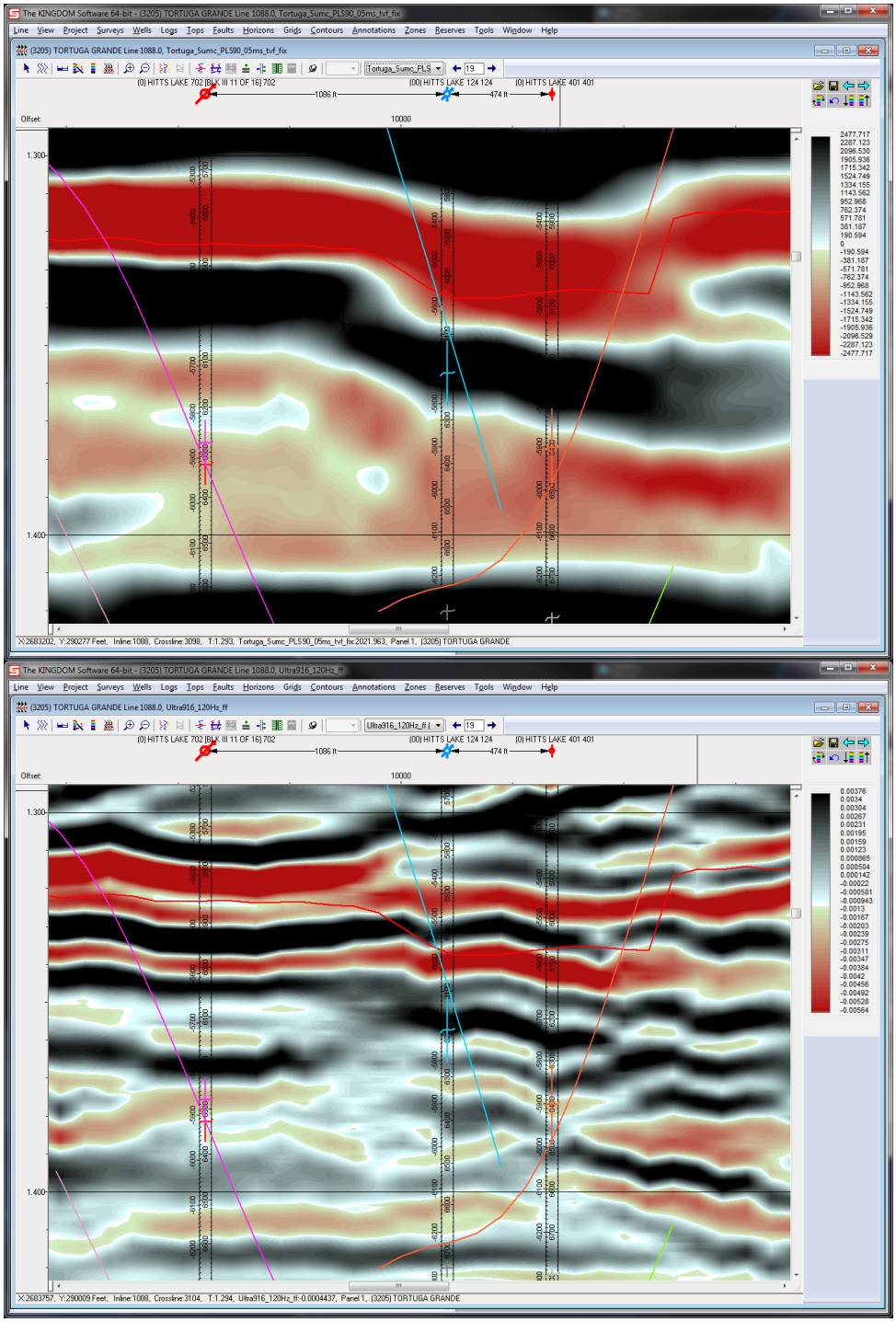

Figure 5.14. A closer view of wells #702, #124, and #401 is shown with seismic (above) and the spectral inversion (below). The faulting colored blue and orange at wells #124 and #401, respectively, are in close agreement with those detected after spectral inversion.

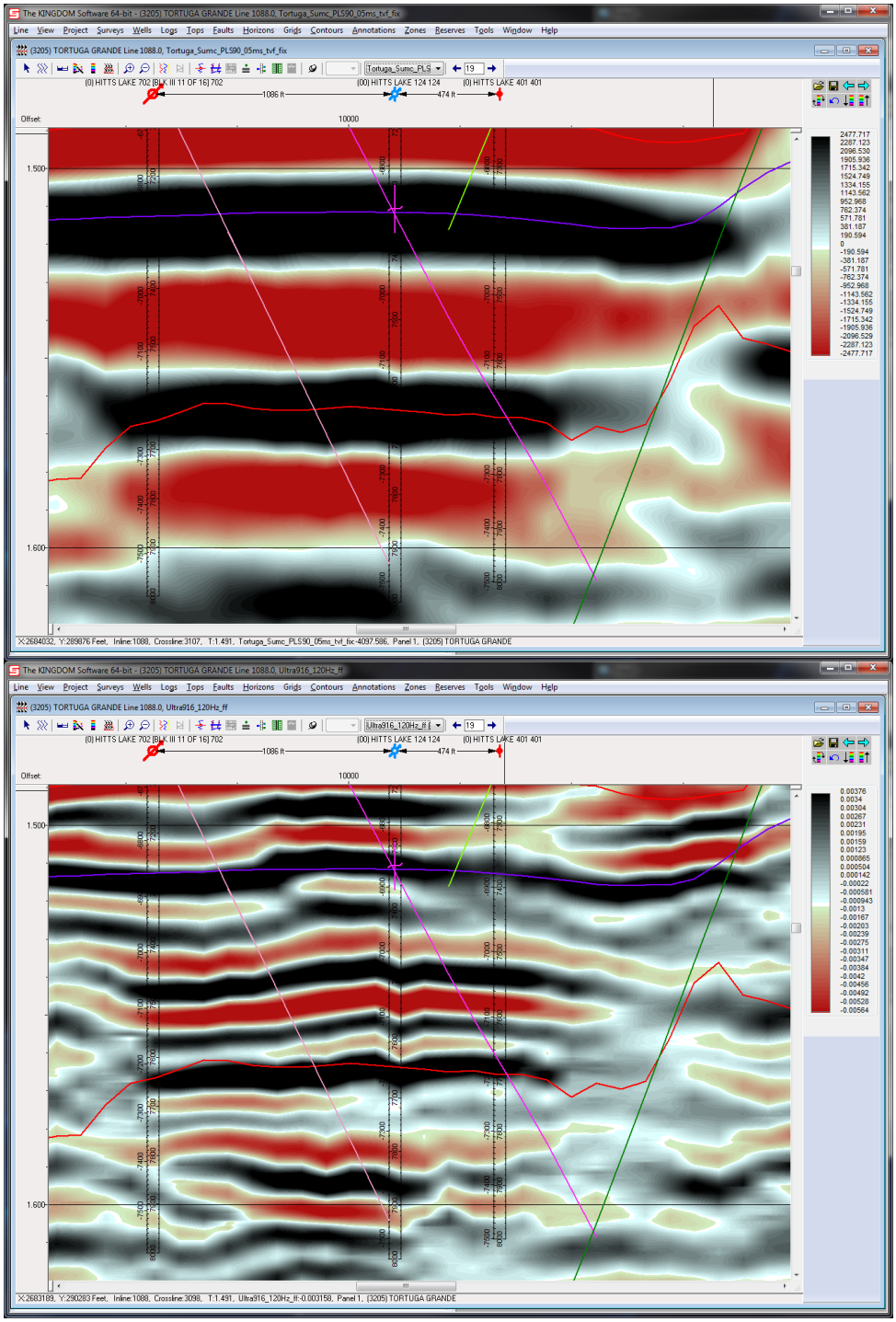

Figure 5.15. A deeper, closer view of wells #702, #124, and #401. The breaks shown follow the log-mapped faulting very well. The pink fault line overlaps the imaged layer only about as much as our lateral resolution: roughly 115 feet (35 m).

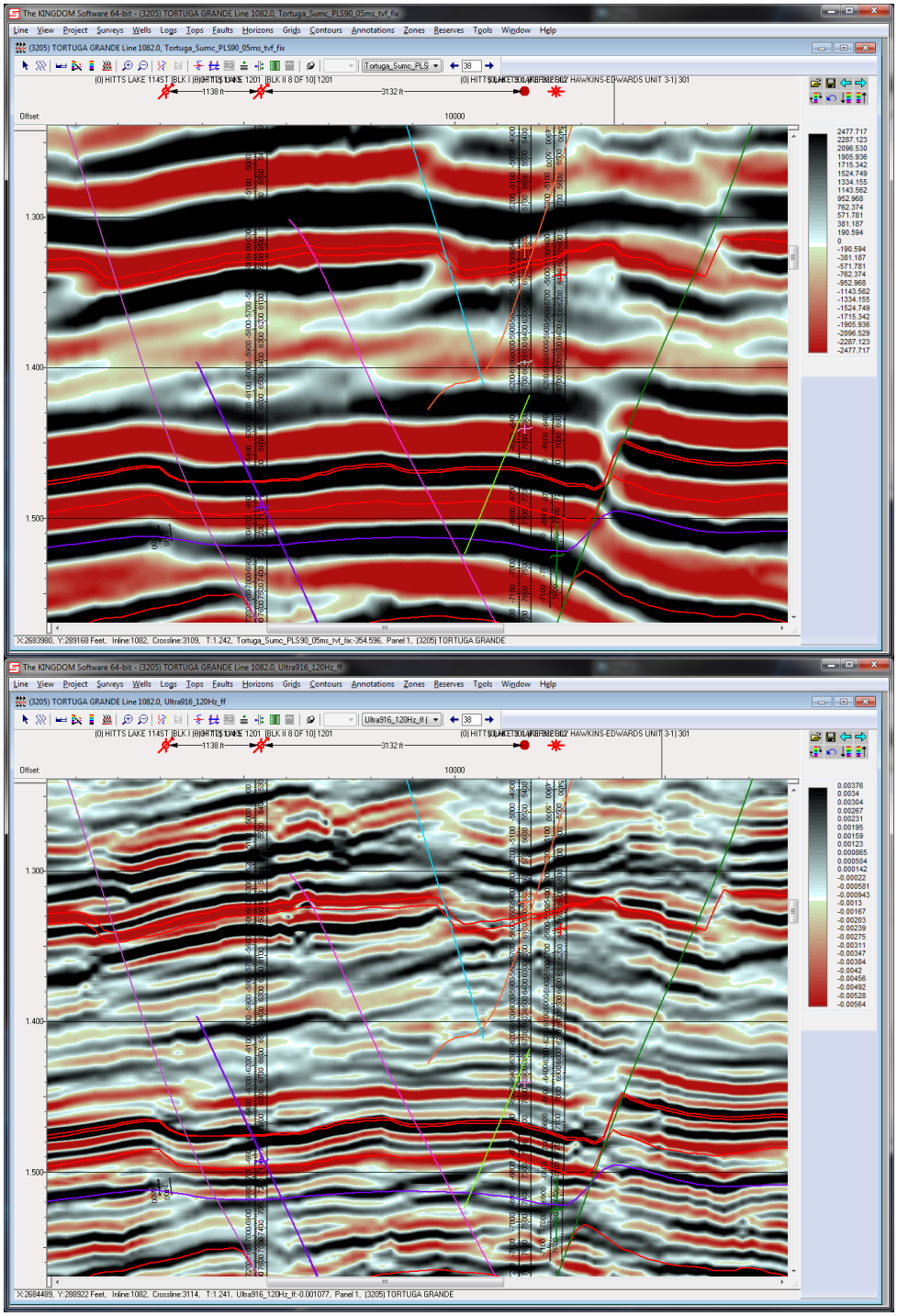

Figure 5.16. A wide view is shown here of wells #1201, #302, and #301. Evidence emerges for the previously undetected green fault. Also, the positions of individual fault cuts agree with the inversion.

The enhanced faulting seen on the spectrally inverted result is commonly at a different dip than those drawn on beforehand during interpretation of the fault cuttings from the well logs.

Chapter 6

Conclusions

Spectral inversion more than doubled the width of the spectrum as compared to the incoming seismic volume over the Hitts Lake Field. Both hypotheses were somewhat satisfied by the results. Firstly, well log synthetics showed good matching against the spectral inversion (SI). Even in cases where the correlation percentage wasn't higher for the SI synthetics, the rating itself was still favorable. Secondly, the SI volume detected several instances of sub-seismic faulting consistent with fault cuts mapped at well locations. Considering that not all faulting with throws above the vertical resolution of the incoming seismic were detectable there either, the encouraging results of the faulting detected after spectral inversion must not be overlooked. While the results here are promising and do, strictly, satisfy the hypotheses made, the received post-stack seismic volume made the majority of time spent on this thesis an exercise in noise filtering. In exploring the spectral inversions generated using different regularization parameters, a somewhat noisier result was accepted in order to retain resolution and detect greater faulting. Future work could include re-processing the pre-stack gathers, if available, to see if any improvements in signal-to-noise ratio can be made.

References

Bigelow, E.L., 1991, Log-derived dip data successfully delineates East Texas Paluxy reservoirs, 32nd Annual Logging Symposium, SPWLA, Symposium Transactions, Paper V.

Castagna, J. P., 2004, Spectral decomposition and high resolution reflectivity inversion: Presented at the Oklahoma Section Meeting, SEG.

Caughey, Charles A., 1977, Depositional Systems in the Paluxy Formation (Lower Cretaceus), Northeast Texas - Oil, Gas, and Groundwater Resources: Bureau of Economic Geology, The University of Texas at Austin, Circular 77-8, 59 p.

Jackson, M.P.A., 1982, Fault Tectonics of the East Texas Basin: Bureau of Economic Geology, The University of Texas at Austin, Circular 82-4, 31 p.

Partyka, G. A., 2005, Spectral decomposition: SEG Distinguished Lecture, (http://ce.seg.org/dl/spring2005/partykaabstract.shtml).

Partyka, G. A., J. A. Gridley, and J. A. Lopez, 1999, Interpretational aspects of spectral decomposition in reservoir characterization: The Leading Edge, **18**, 353–360.

Puryear, C., and J.P. Castagna, 2008, Layer-thickness determination and stratigraphic interpretation using spectral inversion: Theory and application: Geophysics, **73**, no. 2, R37-R48.

Puryear, C., O. Portniaguine, C. Cobos and J. P. Castagna, 2012, “Constrained Least Squares Spectral Analysis: Application to seismic data”: Geophysics, **77**, no. 5, V143-V167 .

Schenk, C.J., and R.J. Viger, 1996, East Texas Basin Province (048) and Louisiana-Mississippi Salt Basins Province (49), U.S. Geological Survey Digital Data Series DDS-30, Release 2, one CD-ROM, 95 p.

Sheriff, R.E., 2002, Encyclopedia Dictionary of Applied Geophysics, 4th Edition: Society of Exploration Geophysicists, p. 370.

Widess, M., 1973, How thin is a thin bed?: Geophysics, **38**, 1176–1180.

Zhang, R., and J. P. Castagna, 2011, Seismic sparse-layer reflectivity inversion using basis pursuit decomposition: Geophysics, **76**, no. 6, R147-R158.